The Sudbury Neutrino Observatory

The SNO Collaboration

J. Boger, R.L. Hahn, J.K. Rowley

Chemistry Department, Brookhaven National Laboratory, Upton, NY 11973-5000 USA [1]

A.L. Carter, B. Hollebone, D. Kessler

Carleton University, Ottawa, Ontario K1S 5B6 CANADA [2]

I. Blevis, F. Dalnoki-Veress, A. DeKok, J. Farine, [3] D.R. Grant, C.K. Hargrove, G. Laberge, I. Levine, K. McFarlane, H. Mes, A.T. Noble, V.M. Novikov, M. O'Neill, M. Shatkay, C. Shewchuk, D. Sinclair

Centre for Research in Particle Physics, Herzberg Laboratory, Carleton University, Ottawa, Ontario K1S 5B6 CANADA [2]

E.T.H. Clifford, R. Deal, E.D. Earle, E. Gaudette, G. Milton, B.Sur

Chalk River Laboratories, AECL Research, Chalk River, Ontario K0J 1J0 CANADA [2]

J. Bigu, J.H.M. Cowan, D.L. Cluff, E.D. Hallman, R.U. Haq, J. Hewett, J.G. Hykawy, G. Jonkmans, [4] R. Michaud, A. Roberge, J. Roberts, E. Saettler, M.H. Schwendener, H. Seifert, D. Sweezey, R. Tafirout, C.J. Virtue

Department of Physics and Astronomy, Laurentian University, Sudbury, Ontario P3E 2C6 CANADA [2]

D.N. Beck, Y.D. Chan, X. Chen, M.R. Dragowsky, [21] F.W. Dycus, J. Gonzalez, M.C.P. Isaac, [5] Y. Kajiyama, G.W. Koehler, K.T. Lesko, M.C. Moebus, E.B. Norman, C.E. Okada, A.W.P. Poon, P. Purgalis, A. Schuelke, A.R. Smith, R.G. Stokstad, S. Turner, [6] I. Zlimen [7]

Lawrence Berkeley National Laboratory, Berkeley, CA 94720 USA [1]

J.M. Anaya, T.J. Bowles, S.J. Brice, Ernst-Ingo Esch, M.M. Fowler, Azriel Goldschmidt, [5] A. Hime, A.F. McGirt, G.G. Miller, W.A. Teasdale, J.B. Wilhelmy, J.M. Wouters

Los Alamos National Laboratory, Los Alamos, NM 87545 USA [1]

J.D. Anglin, M. Bercovitch, W.F. Davidson, R.S. Storey [18]

National Research Council of Canada, Ottawa, Ontario K1A 0R6 CANADA [2]

S. Biller, R.A. Black, R.J. Boardman, M.G. Bowler, J. Cameron, B. Cleveland, A.P. Ferraris, G. Doucas, H. Heron, C. Howard, N.A. Jelley, A.B. Knox, M. Lay, W. Locke, J. Lyon, S. Majerus, M. Moorhead, M. Omori, N.W. Tanner, R.K. Taplin, M. Thorman, D.L. Wark, N. West, J.C. Barton, P.T. Trent

Nuclear and Astrophysics Laboratory, Oxford University, Keble Road, Oxford, OX1 3RH, UK [8]

R. Kouzes, [10] M.M. Lowry [9]

Department of Physics, Princeton University, Princeton, NJ 08544 USA

A.L. Bell, E. Bonvin, [11] M. Boulay, M. Dayon, F. Duncan, L.S. Erhardt, H.C. Evans, G.T. Ewan, R. Ford, [12] A. Hallin, A. Hamer, P.M. Hart, P.J. Harvey, D. Haslip, C.A.W. Hearns, R. Heaton, J.D. Hepburn, C.J. Jillings, E.P. Korpach, H.W. Lee, J.R. Leslie, M.-Q. Liu, H.B. Mak, A.B. McDonald, J.D. MacArthur, W. McLatchie, B.A. Moffat, S. Noel, T.J. Radcliffe, [13] B.C. Robertson, P. Skensved, R.L. Stevenson, X. Zhu

Department of Physics, Queen's University, Kingston, Ontario K7L 3N6 CANADA [2]

S.Gil, [14] J. Heise, R.L. Helmer, [15] R.J. Komar, C.W. Nally, H.S. Ng, C.E. Waltham

Department of Physics and Astronomy, University of British Columbia, Vancouver, BC V6T 2A6 CANADA [2]

R.C. Allen,[16] G. Bühler,[17] H. H. Chen[18]

Department of Physics, University of California, Irvine, CA 92717 USA

G. Aardsma, T. Andersen,[19] K. Cameron, M.C. Chon, R.H. Hanson, P. Jagam, J. Karn, J. Law, R.W. Ollerhead, J.J. Simpson, N. Tagg, J.-X. Wang

Physics Department, University of Guelph, Guelph, Ontario N1G 2W1 CANADA[2]

C. Alexander, E.W. Beier, J.C. Cook, D.F. Cowen, E.D. Frank, W. Frati, P.T. Keener, J.R. Klein, G. Mayers, D.S. McDonald, M.S. Neubauer, F.M. Newcomer, R.J. Pearce, R.G. Van de Water, R. Van Berg, P. Wittich

Department of Physics and Astronomy, University of Pennsylvania, Philadelphia, PA 19104-6396, USA[1]

Q.R. Ahmad, J.M. Beck,[20] M.C. Browne,[21] T.H. Burritt, P.J. Doe, C.A. Duba, S.R. Elliott, J.E. Franklin, J.V. Germani,[22] P. Green,[15] A.A. Hamian, K.M. Heeger, M. Howe, R. Meijer Drees, A. Myers, R.G.H. Robertson, M.W.E. Smith, T.D. Steiger, T. Van Wechel, J.F. Wilkerson

Nuclear Physics Laboratory and Department of Physics, University of Washington, P.O. Box 351560, Seattle, WA 98195 USA [1]

The Sudbury Neutrino Observatory is a second generation water Čerenkov detector designed to determine whether the currently observed solar neutrino deficit is a result of neutrino oscillations. The detector is unique in its use of D_2O as a detection medium, permitting it to make a solar model–independent test of the neutrino oscillation hypothesis by comparison of the charged- and neutral-current interaction rates. In this paper the physical properties, construction, and preliminary operation of the Sudbury Neutrino Observatory are described. Data and predicted operating parameters are provided whenever possible.

Key words: Solar neutrinos, Cherenkov detector, heavy water, He3-proportional counters, water purification
PACS Numbers: 29.40.Ka, 29.40.Cs, 26.65, 14.60.Pq

1 Introduction

The Sudbury Neutrino Observatory (SNO) has been constructed to study the fundamental properties of neutrinos, in particular the mass and mixing parameters. SNO can accomplish this by measuring the flux of electron-type neutrinos, ν_e, which are produced in the sun, and comparing it to the flux of all active flavors of solar neutrinos detected on earth in an appropriate energy interval. Observation of neutrino flavor transformation through this comparison would be compelling evidence of neutrino mass. Non-zero neutrino mass is evidence for physics beyond the Standard Model of fundamental particle interactions [1].

The long distance to the sun makes the search for neutrino mass sensitive to much smaller mass splittings than can be studied with terrestrial sources. Furthermore, the matter density in the sun is sufficiently large to enhance the effects of small mixing between electron neutrinos and mu or tau neutrinos.

[1] Supported by the US Department of Energy.
[2] Supported by Natural Sciences and Engineering Research Council of Canada.
[3] Supported by the Swiss National Science Foundation in 1997.
[4] Present address: Institut de Physique, Université de Neuchâtel, Neuchâtel CH-2000, Switzerland.
[5] Present address: Physics Department, University of California, Berkeley, CA 94720, USA.
[6] Present Address: Penngrove, CA, USA.
[7] Present address: Berkeley, CA, USA.
[8] Supported by Particle Physics and Astronomy Research Council of the UK.
[9] Present address: Physics Department, Brookhaven National Laboratory, Upton, NY 11973 USA.
[10] Present address: Physics Department, West Virginia University, Morgantown WV 26505 USA.
[11] Present address: Membratec, Technopôle, CH-3960 Sierre, Switzerland.
[12] Present address: Department of Physics, Princeton University, Princeton, NJ 08544 USA.
[13] Present address: ESG Canada, 1 Hyperion Ct., Kingston, Ontario, K7K 7G3 Canada.
[14] Present address: CNEA, Av. del Libertador 8250, 1429 Buenos Aires, Argentina.
[15] Permanent address: TRIUMF, Vancouver, British Columbia, V6T 2A3 Canada.
[16] Present address: Hewlett Packard Labs, Mail Stop 4A-D, 1501 Page Mill Road, Palo Alto, CA 94304, USA.
[17] Present address: AT&T, Inc., Middletown, NJ 07748, USA.
[18] Deceased.
[19] Present address: Sienna Software Incorporated, Toronto, Ontario, CA
[20] Present address: Volt Services Group, Seattle, WA 98101, USA.
[21] Present address: Los Alamos National Laboratory, Los Alamos NM 87545, USA.
[22] Present address: WRQ Inc., Seattle, WA 98109, USA.

This matter, or MSW [2], effect also applies when solar neutrinos traverse the earth, and may cause well–defined time and spectral modulations of the signal of ν_e in the SNO detector. Measurement of these effects, made possible by the high counting rate and separable ν_e–specific and flavor–independent responses of the SNO detector, will permit the determination of unique mass and mixing parameters when combined with the existing results of the light-water Čerenkov detectors, ^{37}Cl, and ^{71}Ga solar neutrino experiments [3–5].

The SNO experiment is unique in that it utilizes heavy water, D_2O, in a spherical volume of one kilotonne as a target. The heavy water permits detection of neutrinos through the reactions

$$\nu_x + e^- \rightarrow \nu_x + e^- \quad (1)$$
$$\nu_e + d \rightarrow e^- + p + p \quad (2)$$
$$\nu_x + d \rightarrow \nu_x + n + p \quad (3)$$

where ν_x refers to any active flavor of neutrino. Each of these interactions is detected when one or more electrons produce Čerenkov light that impinges on a phototube array. The elastic scattering (ES) of electrons by neutrinos (Eq. 1) is highly directional, and establishes the sun as the source of the detected neutrinos. The charged-current (CC) absorption of ν_e on deuterons (Eq. 2) produces an electron with an energy highly correlated with that of the neutrino. This reaction is sensitive to the energy spectrum of ν_e and hence to deviations from the parent spectrum. The neutral-current (NC) disintegration of the deuteron by neutrinos (Eq. 3) is independent of neutrino flavor and has a threshold of 2.2 MeV. To be detected, the resulting neutron must be absorbed, giving a 6.25 MeV photon for absorption on deuterium or photons totalling 8.6 MeV for absorption on ^{35}Cl with $MgCl_2$ added to the D_2O. The photon subsequently Compton scatters, imparting enough energy to electrons to create Čerenkov light. (Once the special–purpose neutral-current detectors have been installed, they will provide the primary neutron detection mechanism. See Section 8 for details.) Measurement of the rate of the NC reaction determines the total flux of ^{8}B neutrinos, even if their flavor has been transformed to another active flavor (but not if to a sterile neutrino). The ability to measure the CC and NC reactions separately is unique to SNO and makes the interpretation of the results of the experiment independent of theoretical astrophysics calculations.

All experiments performed to date have detected fewer solar neutrinos than are expected from standard solar models[6]. There are strong hints that this is the result of neutrino flavor transformation between the production point in the sun and the terrestrial detection point. However, these conclusions are based on reference to a calculated prediction. Through direct measurements of the ν_e–specific CC reaction and the flavor–independent NC reaction, the

SNO detector will be the first experiment to make a solar–model–independent measurement of the solar neutrino flux.

SNO can make contributions, some of which are unique, in other areas of physics. An example of the latter is a search for the relic supernova neutrinos integrated over all past supernovae. For the relic supernova neutrinos, the interaction of $\overline{\nu}_e$ on protons in the deuterons produces a Čerenkov signal plus two neutrons, which makes a clean signature. Other topics that SNO will study include the flavor composition of the atmospheric neutrino flux, searches for certain types of dark matter, and nucleon decay. The observatory is designed to handle the high data rates induced by an intense burst of neutrinos from a supernova explosion as close as one kiloparsec away.

An overview of the SNO laboratory and detector is given in Fig.1. The detector consists of a transparent acrylic sphere 12 m in diameter, supported from a deck structure by ten rope loops made of synthetic fiber, as shown in Fig. 2. The sphere holds 1000 tonnes of heavy water. Surrounding the acrylic vessel is a geodesic structure 17.8 m in diameter made of stainless-steel struts and carrying 9438 inward-looking photomultiplier tubes. The barrel-shaped cavity, 22 m in diameter and 34 m in height, is filled with purified light water to provide support and shielding.

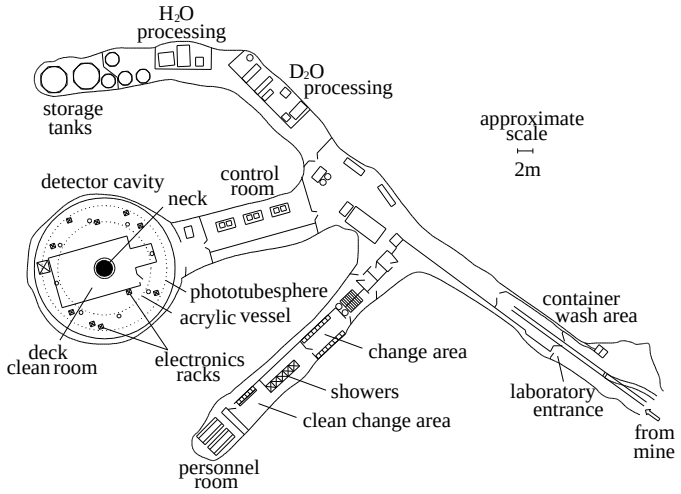

Fig. 1. General Layout of the SNO Laboratory.

The SNO detector is located at 46°28′30″ N, 81°12′04″ W in the INCO, Ltd.,

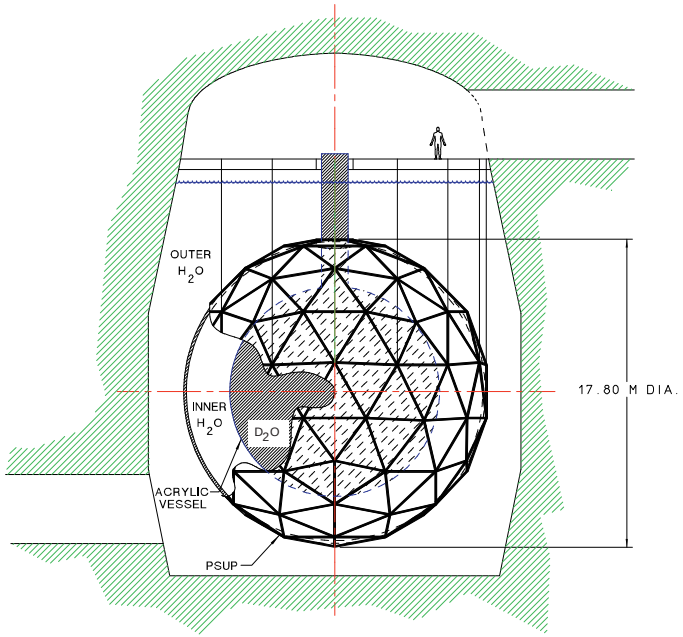

Fig. 2. The PMT support structure (PSUP) shown inside the SNO cavity, surrounding the acrylic vessel, with light water and heavy water volumes located as indicated.

Creighton mine near Sudbury, Ontario, Canada. The center of the detector vessel is 2039 m below the surface in a cavity excavated from the "6800-foot" level of the mine. The surface is 309 m above sea level. The granitic rock overburden (mainly norite) corresponds to approximately 6000 m water equivalent. At this depth, only about 70 muons pass through the detector (inside the photomultiplier array) per day.

The sections below detail the design criteria of many of the important aspects of the detector. The extensive D_2O and H_2O purification systems are described in Section 2 and purity specifications are given there. Since SNO will add high

purity $MgCl_2$ to the D_2O to enhance the NC detection, a description of the system required to handle the heavy water brine is also given. The technically challenging construction of the large acrylic vessel ("AV") which holds the D_2O is described in Section 3. The large array of PMTs and their basic operating parameters are described in Section 4. The materials and construction of the PMT support structure are described in Section 5.

A description of the electronic readout chain is given in Section 6, followed by a description of the downstream data acquisition hardware and software in Section 7. Separate ^{3}He neutral-current detectors, which will be installed at a later date in the D_2O volume, are described in Section 8. The detector control and monitoring system is described in Section 9. The calibration system, consisting of a variety of sources, a manipulator, controlling software, and the analysis of calibration data, is described in Section 10. The extensive effort to maintain and monitor site cleanliness during and after construction is described in Section 11. The large software package used to generate simulated data and analyze acquired data is described in Section 12. Brief descriptions of the present detector status and future plans are in Section 13.

2 Water Systems

The SNO water system is comprised of two separate systems: one for the ultrapure light water (H_2O) and one for the heavy water (D_2O). These systems are located underground near the detector. The source of water for the H_2O system is a surface purification plant that produces potable water for the mine. Underground, the water is pretreated, purified and degassed to levels acceptable for the SNO detector, regassed with pure N_2, and finally cooled before it is put into the detector. Ultrapure water leaches out soluble components when in contact with solid surfaces. It may also support biological activity on such surfaces or on suspended particles. The H_2O is therefore deoxygenated and continuously circulated to remove ions, organics and suspended solids. Both liquids are also assayed continuously to monitor radioactive contaminants.

Incoming potable water contains sand and silt particles, bacteria, algae, inorganic salts, organic molecules and gasses (N_2, O_2, CO_2, Rn, etc.). After falling a total of 6800 feet, the water is supersaturated with air, so first it enters a deaerator tank (see fig. 3) where it spends a few minutes so that some of the dissolved O_2 and N_2 comes out. It then passes into a multimedia filter consisting of a bed of sand and charcoal to remove large particles followed by a 10-micron filter to remove fine particles. The water then enters the laboratory water utility room. A charcoal filter is used to reduce the levels of organic contaminants and to convert free chlorine into chloride since chlorine would damage the reverse osmosis (RO) unit further downstream.

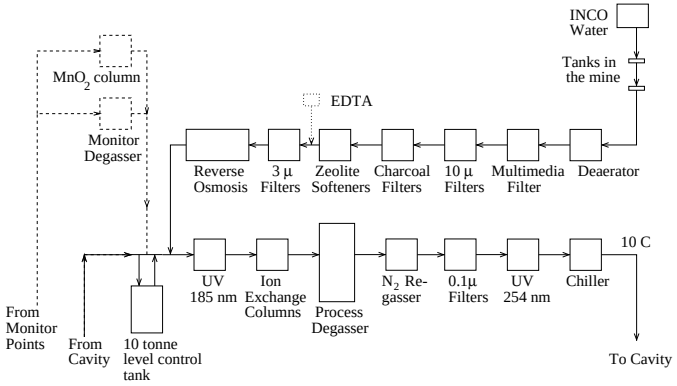

Fig. 3. The light water system.

After the charcoal filter, the water passes into softeners consisting of two 0.14 m^3 bottles containing strong-base Purolite C100-E cation exchange resin. Here divalent ions such as Ca and Mg are exchanged for Na ions. The softeners also remove iron and stabilize colloidal particles so they do not coagulate when concentrated by the RO membranes.

A 9.1% solution of sodium ethylene diamine tetraacetate (EDTA) and sodium bisulphate is injected at 9 ml/min. to complex various ion species (e.g., Al) and to reduce O and Cl into a form that can be rejected by the RO. Then two filter units, each containing twelve 25-cm long, 3-μm filters, remove suspended particles. A silt density index test is done at this point on the running system.

The reverse-osmosis process is the workhorse of the purification system. Twelve spiral-wound thin film composite (polyamide on polysulfone) membranes each 5.6 m^2 in area reduce inorganic salt levels by a factor of at least 20 and reduce organics and hence the EDTA and particles larger than molecular weight 200 with greater than 99% efficiency. The RO performance is monitored online by percentage rejection (typically 97.5%) and conductivity monitors. After the detector is full the RO does not have to be used again unless SNO requires substantial amounts of make-up water in the detector.

After the RO, the water enters a 185-nm UV unit consisting of mercury lamps and quartz sleeves where any remaining organic compounds are broken apart into ionic form. The water next goes to an ion-exchange unit that removes remaining dissolved ionized impurities left by the RO. These are two sets of six bottles in parallel containing 0.1 m^3 of Purolite nuclear grade NWR-37 mixed (cation and anion) bed resins. The exiting water has a resistivity of 18.2 MΩ-cm.

A custom–designed Process Degasser (PD) is used to reduce the O_2 and Rn levels by factors of about 1000 and 50, respectively, in the water [7]. The PD consists of a large electropolished stainless steel vessel (81 cm diameter by 6 m high) containing shower heads, spherical polypropylene packing and heater elements and pumped with a mechanical booster pump (Edwards EH500A) backed by a four-stage positive displacement rotary pump (Edwards QDP80 Drystar). Vacuum is maintained at 20 torr and water vapour flow rate at one kg/hr. The PD removes all gases from the water and can cause, by diffusion, low pressures inside the underwater PMT connectors. Low pressure compromises the breakdown voltage of the connectors, and in a successful effort to reduce breakdowns that occurred with degassed water, the water was regassed with pure nitrogen to atmospheric pressure at the 2000-m depth using a gas permeable membrane unit. This unit is followed by 0.1-μm filters to remove particulates. Then a 254-nm UV unit is used to kill bacteria. Finally a chiller cools the water to 10°C before water is put into the detector at a rate of 150 l/min.

The water mass between the AV and the PMTs is about 1700 tonnes and the mass between the PMTs and the cavity walls is 5700 tonnes. Water enters the detector between the AV and PMTs. Because this region has to be cleaner than the region outside, a 99.99% leak-tight plastic barrier seals the back of the PMTs. Water in the outer region is dirtier due to its large content of submersed material (cables, steel support, cavity liner, etc.). Water is drawn from this region back to the utility room and into a recirculation loop. This loop consists of a ten-tonne polypropylene tank (used by the control loop to maintain constant water level in the detector), the first UV unit, the ion exchange columns, the process degasser, the N_2 regassing unit, the 0.1-μm filters, the second UV unit and the chiller. The recirculated light water is assayed regularly for pH, conductivity, turbidity, anions, cations, suspended solids, dissolved gases, and radioactivity. This is accomplished by means of six sample pipes in the H_2O volume.

The heavy water system is designed to perform the following functions:

- Receive the D_2O and make an initial purification to reduce the amount of contamination reaching the main system;
- Purify the D_2O with or without the $MgCl_2$ additive;
- Assay the D_2O or D_2O brine to make an accurate background determination;
- Manage the addition and removal of the $MgCl_2$ additive on a time scale short relative to the expected running times;

A diagram of the system is shown in Fig. 4.

The source of D_2O was the Ontario Hydro Bruce heavy water plant beside Lake

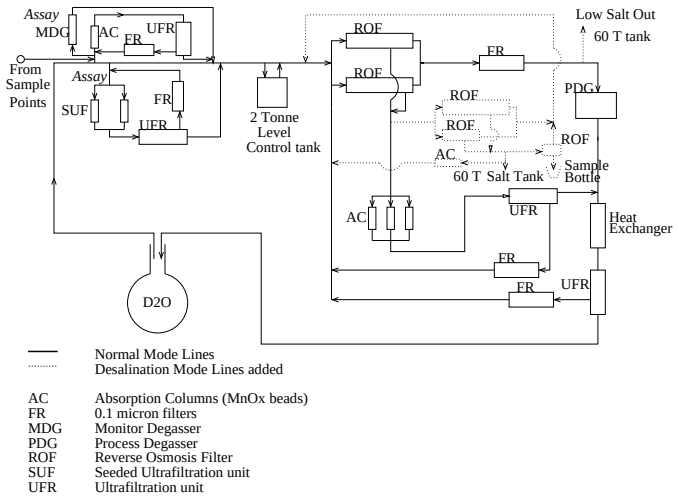

Fig. 4. The heavy water system.

Huron. The D_2O was trucked to the SNO site and transported underground. It was cleaned and stored temporarily before it was put into the acrylic vessel (AV). Heavy water delivered to the lab was first passed through ion-exchange columns to reduce its ionic content, in particular its K content. The D_2O then went into a large polypropylene-lined tank. During the filling of the H_2O and D_2O, the D_2O was filled at such a rate as to maintain zero pressure differential across the bottom of the AV, which assured that the vessel surface was generally in compression.

With the SNO detector filled, the D_2O is recirculated to maintain its purity. This is accomplished by an RO system consisting of five separate pressure housing units and the membranes contained within. Two large (22 cm diameter and 5.5 m length) units are used in parallel for the purification of the recirculating heavy water. The concentrate stream containing the radioactive ions passes through adsorption columns to decrease the Th, Ra and Pb concentrations.

All the water returning to the AV passes through an ultrafiltration unit. This is particularly important following MnO_x and seeded ultrafiltration assays (see below) to insure that fines from these absorbers are not carried into the AV. The D_2O is assayed regularly for density, pH, conductivity, turbidity, anions, cations, total organic carbon and suspended solids. Table 1 gives the isotopic composition of the heavy water.

Table 1
Isotopic composition of SNO heavy water.

Isotope	Abundance	Isotope	Abundance
^{2}H	99.917(5)%	^{17}O	0.17(2)%
^{3}H	0.097(10) μCi/kg	^{18}O	0.71(7)%
^{1}H	Balance	^{16}O	Balance

The D_2O and H_2O have to be isolated from the laboratory air to prevent radon (at a concentration of 3 pCi/l) from getting in, even in the presence of large pressure transients that occur during mine operations. A cover gas system provides nitrogen gas that functions as a physical barrier between the water and the radon-rich laboratory air. The nitrogen comes from the boil-off of liquid nitrogen stored in a 1000-liter dewar. The boiloff gas has been measured to contain less than 10^{-5} pCi radon per liter of nitrogen gas.

Radon in the lab can also enter the water system in other ways. Therefore, when a filter is changed on the D_2O system, radon-free D_2O already in the D_2O system will be used to flush the filter to get rid of trapped laboratory air before bringing the filter back on line. In the H_2O system, H_2O losses from the process degasser, filter changes and small leaks (if any) in the Urylon cavity liner is made up with radon-free water that has been "aged" in a storage tank.

The radioactivity requirements are set primarily by the design goal specifying that the contribution to the neutron-production rate through photodisintegration of the deuteron, with an interaction threshold of 2.2 MeV, should not exceed one-tenth that of the model solar-neutrino rate (5000 y^{-1}). This leads to combined limits of 3×10^{-15}g/g of Th and 4.5×10^{-14}g/g U in the D_2O. SNO's assay systems are expected to have an uncertainty of not more than 20% in their measurement at these impurity levels, although plating may give rise to a systematic uncertainty. There are six sample pipes in various locations inside the AV that allow D_2O samples to be withdrawn for radioassay.

For Th, Ra and Pb assay the seeded ultrafiltration [8] technique (SUF) will be used. The SUF unit contains four large microfilters thinly coated with DTiO. One hundred tonnes of water at a rate of 150 l/min will be passed through them. Then the filters are removed and the Th, Ra, and Pb stripped off and counted. Acrylic beads coated with MnO_x have been shown to be an excellent adsorber for Ra with an extraction efficiency of about 90% [9]. Water is passed at 20 l/min. through a 1-l column containing the MnO_x which is removed off-line for counting of the Ra daughters using an electrostatic device in which charged ions are deposited on the surface of a silicon detector [10].

The number of ^{222}Rn (3.8-d half-life) is measured in six tonnes of liquid taken from one of six regions in the H_2O or one of six regions in the D_2O. The six

tonnes of water are put through a small vacuum degasser [11] at 20 l/min. The gasses which are removed from the water are primarily N_2, O_2, Ar, CO_2 and a few hundred atoms of ^{222}Rn, as well as 10 ml/min in the form of water vapour. Rn is subsequently frozen out in a U-shaped trap cooled with liquid nitrogen (-192 C) and transferred to a ZnS coated scintillation cell [12] for counting.

To enhance the neutral-current detection, $MgCl_2$ will be added to the water to take advantage of the larger neutron-capture cross section of Cl relative to deuterium. A concentration of approximately 0.2% will be used. A D_2O brine solution that has been purified prior to transport underground is put into a large polypropylene lined tank. When it is time to add the $MgCl_2$ to the AV, this tank will slowly be emptied. At the same time, an equivalent volume of salt-free D_2O will be taken out of the AV and put into a second polypropylene lined tank.

To take the $MgCl_2$ out of the AV, the third RO unit will be used in combination with the two main ones to desalinate the water to about 100 parts per million (ppm). In a second desalination pass, a fourth, smaller RO unit will be added to the process to desalinate the D_2O to about one ppm.

3 Acrylic Vessel

The D_2O containment vessel must meet diverse requirements, some of which present opposing design constraints. The primary design criteria for the containment vessel are:

- Isolate 1000 tonnes of D_2O from surrounding H_2O.
- Maintain structural integrity and performance over ten years while immersed in ultrapure D_2O and H_2O and subjected to the seismic activity expected in an operating mine.
- Minimize the total mass of radioactive impurities.
- Maximize optical performance.
- Design for construction in the mine.

The design criteria listed above resulted in the containment vessel shown in Fig. 5.

A 12 meter diameter sphere was chosen as the optimum shape for the containment vessel. A sphere has the largest volume-to-surface ratio, and optimum stress distribution. This reduces the mass of acrylic needed, and hence the amount of radioactivity. The sphere is suspended from ten loops of rope, which are attached to the vessel by means of rope grooves located around the equa-

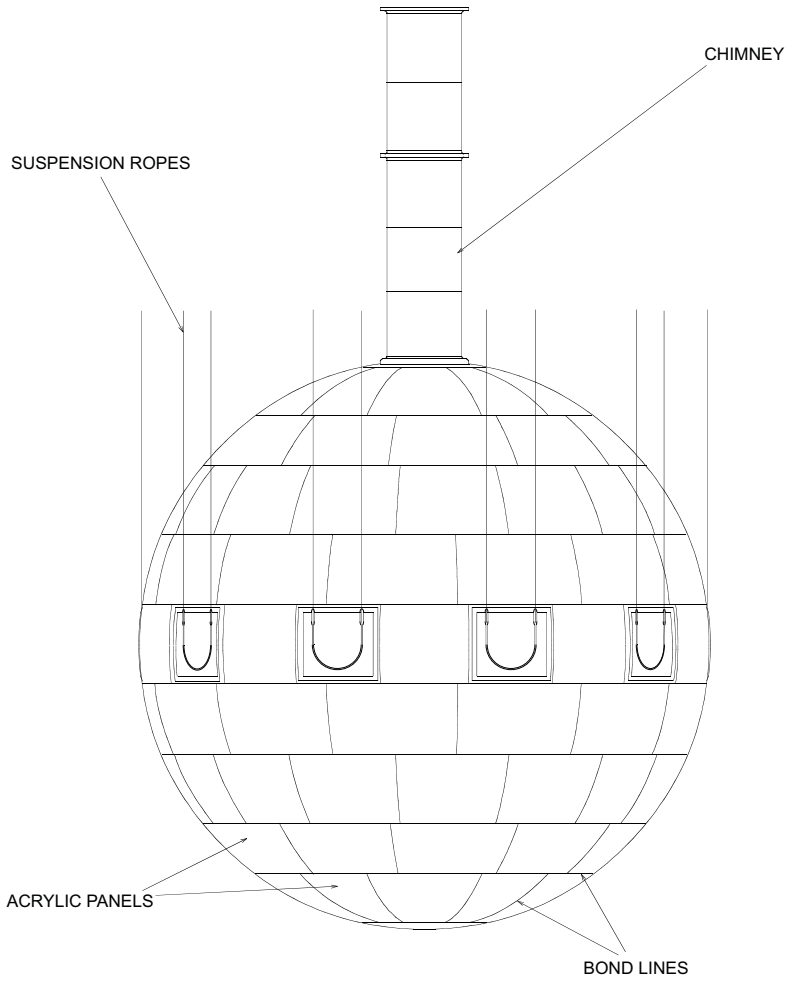

Fig. 5. The SNO acrylic containment vessel.

tor of the sphere. The choice of rope suspension was driven by radioactivity and optical considerations: a rope under tension offers excellent load bearing capacity for a minimum mass, and it presents the minimum obstruction of the

Čerenkov light that neutrino interactions produce.

To allow the insertion of calibration devices and the installation of the ^{3}He neutron detector strings, the sphere is provided with a 1.5-m diameter by 6.8-m tall chimney. Piping also enters and exits the vessel through this chimney. For filling and purification recirculation requirements 7.6-cm diameter pipes introduce D_2O at the bottom of the vessel and remove it from the top of the chimney. D_2O may be extracted via 3.8-cm diameter pipes from four different levels in the vessel and one in the chimney for measurements of both chemical and radioactive water quality.

A total of 122 ultraviolet transmitting (UVT) acrylic panels were used in the construction of the spherical part of the containment vessel. These panels were nominally 5.6 cm thick, with the exception of the ten equatorial panels containing grooves for the suspension ropes. These rope groove panels were nominaly 11.4 cm thick. Acrylic sheet was chosen as the construction material for a number of reasons. A simple hydrocarbon, UVT acrylic can be manufactured with very low intrinsic radioactivity. The light transmission of UVT acrylic matches reasonably the spectral response of the PMTs. Cast acrylic sheet is commercially available in sizes acceptable for mine transportation. It is readily thermoformed into spherical segments and is easily machined. It is capable of being bonded together with bond strengths close to that of the parent material.

The flat cast acrylic panels were first thermoformed into spherical sections by slump forming into a female mold formed from polished aluminum plate with a radius of 6.06 m (the outer radius of the sphere). The panels were then machined to the correct shape on a five-axis milling machine while at a constant temperature of 21°C. To avoid contamination, only clean water was used as a lubricant during machining operations.

A final check of the dimensions was made by "dry assembling" the panels on a special framework to form first the upper hemisphere, then the lower hemisphere. This ensured that all the panels could be fitted together within the specified tolerance of $\pm$25 mm on the spherical curvature required by the buckling criteria. During construction the curvature was typically maintained to $\pm$6 mm.

The panels were bonded together using a partially polymerized adhesive that cures at room temperature. This adhesive was formulated by Reynolds Polymer Technology Inc., the fabricators of the acrylic vessel. The bonds are approximately 3 mm thick and special allowance has to be made for the 20% shrinkage during polymerization of the adhesive. It took considerable R&D and construction time to obtain over 500 m of adequate quality bonds. All bond strengths exceeded 27.5 MPa. Prior to bonding the main vessel the bonding techniques were prototyped by building two small (seven-panel) sections of the sphere.

Table 2
Principal features of the containment vessel (all numbers are at 20°C).

Capacity of sphere	997.91 tonnes of D_2O
Vessel internal diameter	12.01 m
Nominal wall thickness	5.5 cm
Mass of sphere	30.0 tonnes
Capacity of chimney (normal operation)	8.61 tonnes of D_2O
Chimney internal diameter	1.46 m
Chimney height	6.8 m
Mass of chimney	2.53 tonnes
Bulk absorption coeff. of light in acrylic	.01 cm^{-1} @400 nm
	.04 cm^{-1} @360 nm
	.18 cm^{-1} @320 nm

First the upper hemisphere of the vessel was built and the chimney attached. The chimney of the containment vessel was made of five cylinders of ultraviolet absorbing (UVA) cast acrylic to reduce the "piping" of unwanted Čerenkov light from these regions into the inner volume of the detector.

The hemisphere was then raised into its final position and suspended on its ten supporting ropes. Vectran fibers were chosen as the material for the suspension ropes, not only for their low radioactivity but also for their ability to retain strength during long term exposure to ultrapure water. A total of 300 kg of Vectran filament was supplied by Hoechst-Celanese Company. The filaments were twisted into rope by Yale Cordage. Due to the large surface area of the filaments this represents a significant contamination potential due to dust deposition. Therefore the twisting machines were carefully cleaned and tented in plastic prior to use. Each of the ten loops supporting the vessel is approximately 30 m long and 24.4 mm in diameter. In normal operation, each loop is continuously loaded to five tonnes, or approximately 10% of its ultimate strength of 500,000 N.

Working from a suspended construction platform, subsequent rings of the lower hemisphere were constructed and attached to the hanging upper hemisphere. As construction progressed the platform was lowered until the final "south pole" disk was installed.

The principal features of the containment vessel are listed in Table 2.

Table 3
Mechanical measurements of the acrylic panels.

Tensile strength	79 MPa
Tensile elongation	5.05%
Tensile modulus	3.5 GPa
Compressive deformation	0.36%
Residual monomer	1.22%

If acrylic is subject to excessive stress for extended periods of time it will develop crazing cracks which eventually will lead to premature failure. The ten-year design life of the vessel requires that the long-term tensile stresses not exceed 4 MPa. In order to reduce further the tensile stresses, it was decided to place the vessel in compression during normal operation by adjusting the H_2O level with respect to the D_2O level. Optimization of the design was carried out with the ANSYS [14] finite-element analysis code. The structure was studied under a variety of simulated conditions, both normal and abnormal (e.g., with a broken suspension rope). For all these studies it was assumed that the mechanical properties of the bonds were identical to that of the acrylic, an assumption supported by measurements of bonded test specimens.

The Polycast Corp. measured mechanical properties of the acrylic panels to insure that each sheet met design specifications for thickness and mechanical integrity. The averages of five measurements are listed in Table 3. The low percentage of residual monomer listed in the table indicates that the polymerization process is essentially complete and that the mechanical properties of the acrylic will not change.

Stress levels in bonded panels were also recorded by positioning crossed polarisers on each side of the bond and photographing fringes. At the end, the vessel was successfully proof-tested by reducing the internal pressure 7 kPa below ambient pressure to subject the sphere to buckling forces and by pressurizing it to 14 kPa above ambient pressure to subject all the bonds to tensile stresses.

The radioactive and optical requirements for the acrylic were established by Monte Carlo simulation of the detector. To ensure that the acrylic would meet the requirements of the detector, the radioactive properties were measured throughout the supply of materials by means of neutron activation, mass spectrometry, and alpha spectroscopy. Concentrations of Th and U in each acrylic sample were measured to be less than the specified 1.1 pg/g each. For the eleven ropes produced, twelve 2.5-kg samples were taken from the beginning and end of a production run and between each rope. Direct gamma counting yielded upper limits of 200 pg/g Th and U, in agreement with the average value of small-sample neutron-activation results.

Optical absorption coefficients for each production batch of acrylic sheets were measured for samples cut from the sheets. Over 300 measurements were performed. A useful figure of merit is the ratio of the light detected with acrylic to the light detected without acrylic between 300 nm and 440 nm at normal incidence. The figure of merit for the ten thicker equatorial rope groove panels was calculated from the absorption coefficient as if they were 5.6 cm thick. For the 170 sheets manufactured the average figure of merit is 0.73.

4 Photomultiplier Tubes

The primary design considerations for the PMT system are

- High photon detection efficiency,
- Minimal amount of radioactivities in all components, $<$ 120 ng/g U, $<$ 90 ng/g Th, $<$ 0.2 mg/g K,
- Low failure rate for a 10-year lifespan submerged in ultrapure water at a pressure of 200 kPa and for the seismic activity expected at the SNO site,
- Fast anode pulse rise time and fall time and low photoelectron transit time spread, for a single-photoelectron timing resolution standard deviation $<$ 1.70 ns,
- Low dark current noise rate, $<$ 8 kHz, at a charge gain of 10^7,
- Operating voltage less than 3000 V,
- Reasonable charge resolution, $>$ 1.25 peak to valley,
- Low prepulse, late-pulse and after-pulse fractions, $<$ 1.5%,
- Low sensitivity of PMT parameters to external magnetic field: at 100 mG, less than 10% gain reduction and less than 20% timing resolution degradation.

Raw materials from the manufacturers of the PMT components, bases, cables, and housings were assayed for radioactivity [15]. The leach rates of different types of glass and plastic were also measured.

The photomultiplier tubes (PMTs) are immersed in ultrapure water to a maximum depth of 22 m, corresponding to a maximum water pressure of 200 kPa above atmospheric pressure. The failure rate of the PMT components, which consist of the PMT, the resistor chain and the HV/signal cable, must be compatible with the expected approximate ten year detector lifetime. This puts severe contraints on the choice of glass for the PMT envelope, the shape of the envelope, the type of cable, and the design of the waterproof enclosure that protects the resistor chain. Raw materials from all manufacturers were assayed for radioactivity [15]. The dominant contributor to the contaminant content of the PMT is the glass which has a mass of 850 g and Th and U impurity levels of roughly 40 ppb. The leach rates of different types of glass

and plastic were also measured.

Following detailed stress analysis of the proposed glass envelopes, a mushroom shaped envelope was judged to be most suitable for this underwater application and least likely to deteriorate under long term hydraulic pressure in UPW. Schott Glaswerke produced a new borosilicate glass (Schott 8246) for SNO. The Th and U impurities in this glass are less than 40 ppb. Its water resistance is rated as class 1 (same as Pyrex). In addition, this glass has outstanding optical transmission properties at short wavelengths, with a bulk light absorption coefficient of better than 0.5 cm^{-1} at 320 nm wavelength, and low He permeability. Schott refitted a furnace with a special low-radioactivity liner to produce 16000 mouthblown bulbs for SNO and the LSND Project[16].

The most important PMT parameters are the noise rate, the efficiency, the transit-time spread and the amount of K, U and Th in each PMT. The energy resolution and the event vertex spatial resolution are largely determined by the first three parameters and the detector energy threshold is strongly affected by the radioactivities in the PMT components.

The Hamamatsu R1408 PMT was selected for use in SNO. A schematic drawing of the R1408 is shown in Fig. 6. From the measured U and Th concentrations in the internal parts and glass envelope, the total weight of Th and U in each PMT is estimated to be about 100 μg, about a factor of 14 below specifications. The 9438 inward facing PMTs collect the Čerenkov photons, providing a photocathode coverage of 31%. To improve the light collection efficiency, a 27 cm diameter light concentrator is mounted on each PMT, increasing the effective photocathode coverage to about 59%. The reflectivity of the concentrator reduces this figure to 54%. Of the inward facing tubes, 49 have a dynode tap and a second signal cable. These "low gain" channels extend the dynamic range of SNO at high light intensities by about a factor of 100. Another 91 PMTs without concentrators are mounted facing outward to detect light from muons and other sources in the region exterior to the PMT support structure.

The PMT anode is at positive high voltage, typically in the range 1700 V to 2100 V, and the photocathode is at ground voltage. A single RG59/U type cable is used to carry the high voltage and the fast anode pulse which is capacitively coupled to the front-end electronics. The primary concern in selecting materials for the resistor chain circuit board is radioactivity. Each two-layer Kapton circuit board, with surface mounted components and a through-hole 0.0047-μF film capacitors for filtering and source termination, contains a total of about 2 μg of thorium and 0.6 μg of uranium, about a factor of five lower than the design goal.

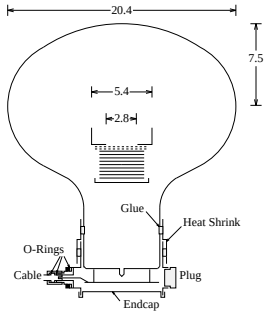

Fig. 6. A schematic of the Hamamatsu R1408 PMT and its waterproof enclosure. The 9 dynodes are shown as solid horizontal lines. The focusing grid is shown as the dashed lines above the dynodes. The volume inside the enclosure is filled with soft silicone gel. The end cap is flexible to allow for thermal expansion. The plug is sealed with heat shrink and thermal adhesive. Dimensions are in cm.

The main function of the waterproof enclosure is to keep the PMT base dry when the PMT is deployed under water. There are two water barriers protecting the circuit board to ensure a low failure rate. The outer enclosure consists of a plastic housing, waterproof modified "TNC" connector and heat shrink tubing with thermal adhesive. (A connector was used to simplify construction and cabling.) The shrink tubing and adhesive are used to hold the plastic housing onto the PMT. The cavity inside the enclosure is filled with a silicone dielectric gel (GE RTV6196) which acts as the second water seal. The silicone gel contains less than 23 ng/g of Th and less than 12 ng/g of U. The polypropylene plastic housing contains less than 10 ppb of Th and less than 6 ppb of U. The heat shrink tubing is made of clear polyolefin which has low Th and U impurities. The TNC connector was provided by M/A-COM with modifications specified by SNO. These connectors exhibited breakdown at nominal high voltage settings, a problem which was overcome by the addition of nitrogen gas to the water, as described in the previous section. Heat shrink and thermal adhesive seal the cable to the male connector.

The RG59/U type cable was designed by Belden, Inc. for SNO. It consists of a copper clad steel central conductor surrounded in succession by 1.85 mm thick solid polyethylene dielectric, 95% tinned copper braid, Duofoil bonded metallic shield and 1.3 mm thick high-density polyethylene outer jacket. The colouring compound mix in the outer jacket is reduced to 0.1% carbon black, the minimum amount needed to make the jacket opaque. Each PMT cable is 32 m long and contains between 10–17 μg of Th and a few μg of U. The

attenuation at 400 MHz is 7.3 dB/30.5 m. The delay is 4.9 ns/m.

The Hamamatsu R1408 PMT has unusually stable gain characteristics with respect to the influence of weak magnetic fields [17]. In the SNO detector the earth's magnetic field is about 55 μT and points approximately 15 degrees off the vertical axis. In such a field, the photon-detection efficiency average over all the PMTs would be about 82% of the detection efficiency at zero magnetic field. Because the PMT efficiency is reduced by less than 3% at magnetic field intensities of 20 μT, only the vertical component of the magnetic field in the SNO detector is cancelled with 14 horizontal field-compensation coils embedded in the cavity walls. With the proper currents, the maximum residual field in the PMT region is 19 μT, and the reduction in photon-detection efficiency is about 2.5% from the zero-field value.

The single photoelectron test system and test results are described in detail in refs. [18,19]. A total of 9829 PMTs passed the acceptance test. The average RMS timing resolution is found to be 1.7 ns, in line with the specification. The mean relative efficiency, defined in Ref. [18], is 10% better than specification. The mean noise rate is 2.3 kHz at 20°C. The cooler temperature in the detector (approximately 10°C) reduces the mean noise rate to approximately 500 Hz, including signals due to residual radioactivity in the detector. The mean operating voltage is 1875 V.

5 Photomultiplier Tube Support Structure

The photomultiplier tubes, their light concentrators and associated hardware are collectively referred to as the PMT Support Structure or the PSUP. The geometry of this platform is fundamentally established by maximizing photon collection while minimizing background signals, fabrication costs, complexity, and transportation and installation intricacy. The D_2O target geometry, the PMT specifications, light concentrator performance, and cavity geometry all affect the final PSUP configuration.

The PSUP serves the additional function of providing a barrier between the core of the experiment (the D_2O target and light collection surfaces) and the outer regions of the experiment. This barrier shields the PMTs from light generated in the outer regions of the experiment. These regions include the cavity walls and the support piping and cabling for the experiment. Near the cavity walls the radioactivity in the surrounding rock creates a significant photon background. The complexity of the cabling and piping makes the outer region difficult to clean and keep clean during construction and the radioactive purity of the materials needed for some of these functions could not be reasonably controlled to the same levels as other detector components. The PSUP also

functions as a highly impermeable barrier to waterborne contamination, ensuring that the highly purified water in the sensitive region between the PMTs and the AV is effectively isolated from the dirtier water in the outer regions.

The PSUP also supports the outward looking PMTs, LED calibration sources, and water-recirculation and monitoring piping.

The design criteria for the PSUP include:

- Maximizing the collection of optical signals from the D_2O target while minimizing a variety of background sources;
- Maintaining performance and integrity of the array, with no required maintenance, for at least a ten year span submerged in ultrapure water and for a variety of seismic conditions anticipated at the SNO site;
- Minimizing the mass of the components to reduce intrinsic backgrounds;
- Producing and fabricating the array from documented low radioactivity materials;
- Maintaining a high impermeability water barrier between the inner and outer light water regions;
- Maintaining an effective barrier to light generated in the outer regions;
- Minimizing the complications of transporting and installing the array at the underground site;
- Producing and fabricating the array from materials inimical to biological growth with low leaching characteristics, low magnetic susceptibility and low electrolytic characteristics;
- Utilizing materials and installation processes compatible with the underground (mining) environment;
- Installing the upper half of the geodesic sphere and supporting the loads of roughly half the detector array during which time the AV is constructed.

The PSUP is logically viewed as two systems–a geodesic sphere that functions as the main support system and the panel arrays that house the PMTs and concentrators. The geodesic sphere, an 889-cm radius three-frequency icosahedron, is shown in Fig. 2. Normally this geodesic sphere would utilize 92 nodal connections between the 270 struts. This choice of geodesic structure uses three different strut lengths with similar linear dimensions. The topmost node is replaced with a hollow toroidal ring and the connecting struts shortened to accommodate the acrylic vessel chimney. Additional toroidal rings guide the acrylic vessel support ropes through the PSUP. Ninety-one outward viewing PMTs are supported on the PSUP struts. The design of the geodesic sphere and panel arrays is fully documented [20].

The geodesic sphere is suspended on 15 stainless steel wire rope cables from the cavity deck. These cables terminate in a spherical thrust bearing on the deck and are monitored with load cells. The position of the array is adjustable

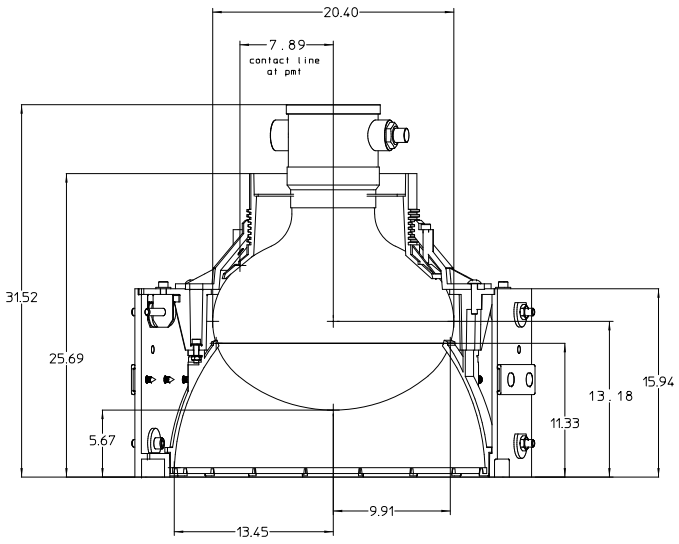

Fig. 7. Photomultiplier mounted in a hexagonal ABS cell, which also forms the light-concentrator housing. Dimensions are in cm.

in the z-direction (up-down) by ± 10 cm. When submerged, the array becomes buoyant, and is therefore secured to the cavity floor at a set of anchor points, each with a pulley and cable that attaches to the main PSUP suspension brackets.

Wire rope cannot effectively be manufactured without lubrication. The main suspension cables are plastic coated and encased in an additional plastic housing to prevent contamination of the water. Anchor cables are plastic coated.

The PMTs are secured in hexagonal ABS (Acrylonitrile-Butadiene-Styrene) black plastic housings that also support light concentrators (reflectors) for each inward-looking PMT [21] as shown in fig. 7.

The concentrators increase the effective area of the photocathode to maximize the number of photons detected, and limit the angular acceptance of the photomultipliers so that only the central part of the detector (where backgrounds are lowest) is in view. They are designed with a three-dimensional critical angle of 56.4°, which means the detector is viewed by each PMT out to a radius of 7 m. The increase in light collection efficiency is approximately 75% [21].

A concentrator is made of 18 pieces of thin dielectric-coated aluminum sheet

curved and placed around the holder of ABS plastic. The optically active coating consists of a layer of specular aluminum covered by a low refractive index layer of magnesium fluoride, which is in turn covered by a high refractive index layer of mixed titanium and praeseodymium oxides. The coating thicknesses are optimized to maximize reflectance in water over the visible and near-UV range of wavelengths, and over a wide range of incident angles. The mean effective reflectance in water is 82±3%.

The top dielectric layer also forms a protective barrier against corrosion in water and was applied to the back exposed surface of the aluminum pieces as well. A protective layer of titanium oxide was applied to the edges. The material was subjected to extensive aging prior to construction. It was found to have a useful life of many years under deoxygenated deionized water with a pH around 7, the normal environment in SNO.

The hexagonal PMT assemblies are collected together into flat arrays of between 7 and 21 PMTs to form a set of repeating arrays used to tessellate the spherical surface of the geodesic structure. Each panel array is secured to the geodesic structure with three adjustable mounts. These mounts permit the delicate panel arrays to accommodate the geodesic structure struts flexing under changing load conditions (most notably, when going from a fully instrumented dry array to a fully submerged array). This alignment is critical to ensure that each PMT views the full D_2O volume. A total of 751 panel arrays tessellate the sphere providing 9522 hexagonal cells. Of these locations, the final design used 60 cells to accomodate the 20 AV ropes and six to provide access at six locations for calibration sources preserving the optical and water flow requirements for the array. During the water fill 18 PMTs were removed for diagnostic testing and their locations appropriately capped, leaving 9438 cells occupied with PMTs. The hexagonal cells cover $\sim$ 85% of the surface area of the geodesic sphere.

Water piping and sampling tubes as well as several pulsed blue LED calibration devices are accommodated in the small spaces between PMT panel arrays.

The PMT support structure is subjected to a variety of loading conditions and stresses. Exposure to ultrapure water is known to reduce the mechanical performance of many materials over time. The design is optimized with the criteria listed above with both hand calculations and a detailed ANSYS finite element analysis of the PSUP under a variety of conditions. A half-scale model, partial full-scale model and dry fit-up of the entire geodesic sphere were used to confirm the design.

The analyses (both stress and buckling) study numerous effects, such as the variation of mechanical and physical properties with time and immersion in

water, the effects of water fill on the deflections and stresses in the PSUP in order to establish acceptable filling-rate limits, the consequences of one of the PSUP supports failing, the effects of various construction tolerances, and the response of the natural frequency of the PSUP under dynamic conditions [22].

Various stainless steel alloys are used in the fabrication of the geodesic sphere and panel arrays, primarily SS304L for welded components and SS304 for parts that are only machined. These alloys have an excellent documented history of long-term exposure to deionized (ultrapure) water. Welding was accomplished with inert-gas processes. A vacuum-deposited Ag coat provides a clean anti-galling agent for threaded fasteners without compromising water purity.

In order to reduce the likelihood of stress corrosion and cracking, plate and tube material is pickled and passivated. Steel fasteners are fabricated from raw materials meeting the same specifications and are in addition heat-treated and quenched.

ABS plastic is used in the injection molded components of the PMT housings. General Electric resin GPX5600 color 4500 was selected for the molding. This selection of plastic provides excellent impact, thermal, chemical resistance, and injection molding characteristics. Since ABS plastic has a limited documented history of exposure to deionized water, we conducted extensive accelerated aging tests to confirm the behavior of the ABS GPX5600 to long term ultrapure water exposure and to insure an adequate safety factor for the design life[23]. Plastic components were injection molded using controlled raw materials and processes. The machines were thoroughly cleaned prior to and during the fabrication cycle of the components. The assembly areas were tented and machine operators used clean gloves during the production of the items.

Radioactivity of all components or samples of raw materials used in the fabrication of the PSUP were subjected to direct counting to determine U and Th concentration. Specified limits of 15 ng/g for each of these species are met by all materials; measured upper limits are typically a factor of 3 to 5 times lower. All clean components were stored in clean plastic bags prior to assembly. Assembly of the PSUP components was accomplished in cleanroom assembly areas with conditions typically better than Class 1000. Assembled components were stored in clean plastic bags prior to installation.

6 Electronics

The electronics chain is required to provide sub-nanosecond time and wide-dynamic-range charge measurement for the PMT pulses. While the solar neu-

trino event rate is very low, the electronics chain must handle background rates in excess of 1 kHz and burst rates from potential supernovae in excess of 1 MHz without significant deadtime. The chain is implemented using three full custom, application specific integrated circuits (ASICs) and commercial ADCs, memory, and logic. The Data Acquisition (DAQ) interface is VME compatible. The ASICs carry out virtually all the analog signal processing and part of the digital signal processing. The ASIC chip set consists of a wide-dynamic-range integrator, a fast and sensitive discriminator/gating circuit, and an analog/digital pipelined memory with a timing circuit. The use of these ASICs provides increased reliability and decreased per-channel cost. Further cost reduction and improved functionality is obtained by using high-volume, large-scale-integration commercial components for the remainder of the circuitry, including numerous field programmable gate arrays (FPGAs).

The signal processing electronics occupies 19 crates, each processing signals from 512 PMTs. The signal and high voltage for each PMT are carried on a single cable and connected in groups of 8 at the rear of each crate to one of sixteen PMT interface cards (PMTICs). The signal then enters one of sixteen front-end cards (FECs), where it is processed by the custom ASICs. The ASICs reside on four daughter boards (DBs), each of which handles 8 channels. One FEC processes 32 channels, digitizes the signals, and stores the digital results in 4 MB of on–board memory, large enough to buffer event bursts (roughly speaking, the memory in all the FECs could hold a one-million-event supernova burst). The FECs are attached to a custom backplane ("SNOBus") that implements the SNO signal- and power-distribution protocol. Also attached to the backplane are a translator card and a trigger-formation card. The XL1 translator card operates in conjunction with a companion XL2 translator card in the DAQ VME crate to communicate with the single-board embedded processor (eCPU) of the DAQ VME crate downstream (see Section 7). The trigger card and the associated trigger system are described below. Programmable test, calibration, and diagnostic facilities are implemented throughout the crate. An overview of the full system is provided by Fig. 8.

The analog part of the chain, from PMT to ASIC chip set, operates as roughly 9500 independent, asynchronous, data-driven pipelines. The subsequent readout part of the chain operates as a separate, clock-driven system that moves the data from the FECs to the DAQ VME system. Each element of the chain is described below.

The analog pulse from each PMT travels through 32 m of 75Ω RG59-like waterproof coaxial cable to the PMTIC. One commercial high-voltage power supply provides about 70 mA DC for the 16 PMTICs (512 PMTs) in one crate. Current to the PMTs passes through individual isolating, filtering, and trimming networks. The PMTIC plugs into the rear of the SNOBus crate and connects directly to its companion FEC in the front of the crate. The PMTIC

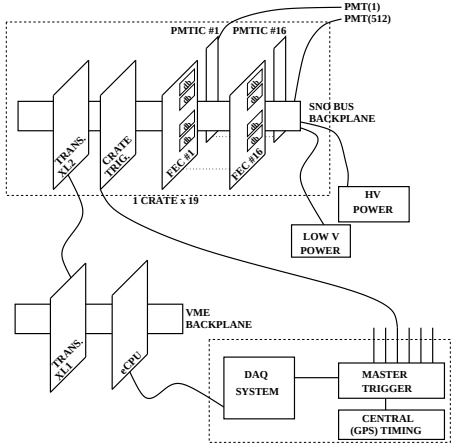

Fig. 8. Overview of the SNO custom data acquisition electronics.

also provides disconnects for individual cables, HV blocking capacitors for the PMT signal, overvoltage and breakdown protection for the integrated circuits, limited readback of the PMT current, and a programmable calibration pulse source for each channel. The PMT signal is transmitted through a connector to the FEC where it is properly terminated, split and attenuated.

On the FEC, the signal current is delivered to one of four daughter boards. The DBs physically separate most of the analog signals from most of the digital signals in order to reduce potential crosstalk, and simplify the overall FEC+DB design. The signal is then fed to a four-channel discriminator chip (SNOD) where any leading edge is observed by a fast differentiator. The current is split into two branches (approximately in the ratio 1:16) and fed into two separate channels – one low gain, the other high gain – of an eight-channel charge integrator (SNOINT). The SNOD and SNOINT chips were fabricated as custom designs in AT&T's CBICU-2 process [24,25]. The SNOINT chip, which uses high-quality external capacitors for the actual integration, has dual integrator channels in order to increase the effective dynamic range to more than 14 bits. The SNOINT also provides shaped low and high gain analog sums of the PMT input signals for use in detector triggering. Each channel of the SNOD chip has independent discriminator and gate generators to provide the timing functions necessary for the SNOINT chip. A timing diagram for the SNOD and SNOINT chips is shown in Fig. 9. The SNOINT and SNOD chip outputs are then delivered to the CMOS ASIC analog memory.

The CMOS member of the SNO chip set (QUSN7) provides analog memory,

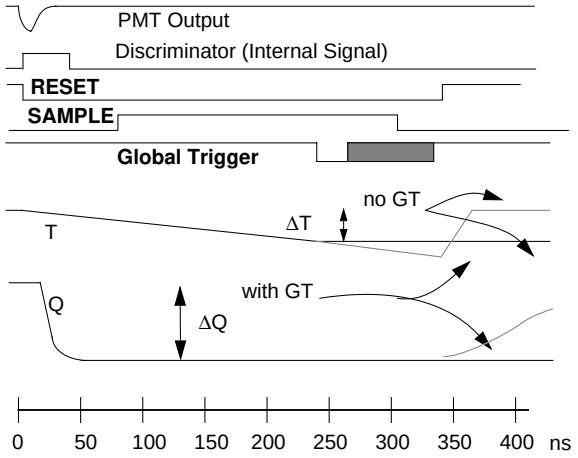

Fig. 9. Single channel timing cycle. With no GT present, a channel resets automatically at the end of a timing cycle ($\sim$ 400 ns).

a time–to–amplitude converter (TAC), and channel and trigger logic for the SNO detector. The 16–deep memory samples the low- and high-gain channels of the SNOINT at early and late times, for a total of four possible charge samples [26]. The QUSN7 chip also receives a signal from the SNOD which is used to initiate a time measurement cycle and the creation of system trigger primitives. These single-channel trigger primitives constitute the first stage of a 9438-input analog sum. This mixed analog/digital device uses custom analog blocks combined with auto-placed and routed standard cells and is fabricated in the Northern Telecom CMOS4S process [27].

The timing sequence and TAC in QUSN7 are initiated on the leading edge of a signal from SNOD. The TAC for a given PMT is started whenever that PMT fires, and is either stopped by a centrally generated Global Trigger (GT) signal or resets itself if no GT arrives after an internal timeout period. On a valid GT, four analog voltages (corresponding to one time and three of the four selectable charge measurements) are stored in one of the 16 analog memory banks, an associated digital memory records the sequence number of the GT (for event building), the memory location (for second order corrections of the data) and any associated condition flags, and a data-available flag is set. The overall trigger deadtime is less than 10 ns, and since each channel is self-resetting, the only other relevant deadtime is the *per PMT* deadtime, which

is set to about 400 ns to allow for light reflection across the SNO detector volume. These two contributions to the detector deadtime are negligible.

The QUSN7 chip also generates two trigger primitive signals, a short coincidence (roughly 20 ns) and a long coincidence (roughly 100 ns), some basic utility functions, and extensive self-test capability. Separate internal counters are used to keep track of PMT noise rates and count error conditions. All counters and latches are accessible for testing via an external scan path and a variety of programmable adjustments are built in.

A data available flag from any QUSN7 initiates an external 32–channel readout sequencer. The sequencer is a clocked, synchronous state machine implemented in a standard field-programmable gate array (FPGA). At the sequencer's convenience, a QUSN7 chip with available data is selected and presents four individually buffered analog voltages to the four on-board 12-bit 2-μs ADCs. After the ADCs have sampled the analog voltages, the sequencer reads three bytes of digital information: the 16-bit GT sequence number, four bits of cell address, and four flag bits. A fourth read strobe clears the memory location.

At the end of the sequencer's cycle, a 3-word, 12-byte, fixed-format data structure is loaded into the on–board memory. The memory is a standard SIMM DRAM under the control of a commercial dual port controller. The sequencer operates one port of the controller as a FIFO while the second port is accessed via the downstream DAQ interface. Each three word descriptor is complete in the sense that the measured time and charge and the geographic channel number and temporal GT sequence number are fully specified, so while it is possible that hit descriptors will be loaded into memory out of temporal sequence, they can be properly sorted out in the downstream DAQ event builder.

The pair of translator cards (XL1, XL2) implements a high speed ($>$ 8 MB/s) RS485 link between each SNOBus crate and the central DAQ VME crate (shown in Fig. 8 containing a Motorola 68040 single-board computer, or "embedded CPU" (eCPU)). The translator card located in the SNOBus crate performs a TTL$\leftrightarrow$GTL conversion. The use of GTL (Gunning Transceiver Logic, with a 0.8-V swing) on the SNOBus backplane for all data, address and control lines reduces the possibility of crosstalk with the sensitive, low voltage PMT signals. For the same reason, clock, DTACK (the VME data handshake signal) and other important signals are transmitted on the SNOBus backplane as low–level single–ended emitter-coupled logic. All signals are terminated, and the use of a 2-mm grid, 165-pin connector on this custom backplane makes for a more compact and flexible system and permits the use of a greatly increased number of ground lines relative to standard VME.

Each MeV of energy deposited in the SNO detector is expected to result in

roughly eight contemporaneous photoelectrons detected by the PMT array. Thus the most powerful hardware trigger for detection of solar neutrinos is a simple count of the number of PMTs that have fired in the recent past. Because the PMT array is 17 m in diameter, different photons from an interaction in the D_2O could differ in travel time to the PMTs by as much as 66 ns (or longer, if they undergo reflection(s)). For this reason the trigger resolving time is set digitally to about 100 ns to allow all unreflected photons from a Čerenkov event to be counted toward a possible trigger. The actual counting of hits is done via a chain of analog summations.

A signal from SNOD is used in QUSN7 to initiate a pair of independent current pulses. The longer pulse (nominally 100 ns) is sent to the first stage of a 9438-input analog sum. Summations at the FEC, crate, and full detector level follow. The final summation is compared against a programmable threshold, and a sum above this threshold will generate a GT. The second current pulse generated by QUSN7 is nominally much narrower (about 20 ns), has a digitally set width and delay and, in an identical summing tree, generates a separate trigger useful for studies in which one wishes to scrutinize a selected, smaller, fiducial volume of the detector.

In addition to these two discrete analog sums, the SNO trigger system can trigger on the analog sum of the 9438 shaped PMT signals produced by the SNOINT chips, and copies of each of the sums are sent to a digital oscilloscope for real time monitoring of the state of all 9438 channels. For the 100 ns coincidence trigger, up to three separate thresholds can be set simultaneously, and triggers from the lowest threshold can be prescaled with a factor as large as 65,534 to provide a monitor of very low energy backgrounds. A built-in pulser provides a "pulsed–GT" trigger, which is used as a "zero bias" trigger for the detector. All trigger types can be enabled simultaneously, and bits corresponding to each type that fired in a given event are latched in a "trigger word" that is part of the data stream.

Two separate oscillators are used to keep a record of absolute and relative time. A commercial GPS system provides a 10 MHz signal as well as precision time markers at requested Universal Times. This system is nominally accurate to order 100 ns and will allow correlation of SNO data with that of other astronomical detectors. Since the GPS receiver must be on the surface and all the other electronics is below ground, communication delays due to the 4 km long fiber optics must be continuously monitored. This is done by using a separate fiber in the same bundle and measuring total round trip propagation time. A highly stable quartz oscillator operating at 50 MHz offers a higher precision inter–event timing standard.

Extensive measurements have been made of the electronics all the way from the integrated circuits to the full operating 9728 channel system (19 crates with

512 channels each, a number of which are connected to non-PMT sources) which had been installed underground and was completely operational by the spring of 1998. Tests of the front end custom ASICs running as single devices, as a coupled chip set, and on full functionality production boards running with the prototype and then production DAQ software were very successful. The performance of the bipolar chips is very close to that predicted in the pre-fabrication simulations and the CMOS chip is adequate for the experiment. The charge linearity fully satisfies our design goals. The linearity and precision of the time measurement are also significantly better than the minimum requirements of SNO. Tests with pulsers and actual SNO PMTs have verified stable and reliable operation of the chip set and the system even under the unanticipated challenge of high rate full voltage breakdowns in degassed H_2O at some of the underwater PMT connectors. A single-photoelectron spectrum with no discriminator threshold set is shown in Fig. 10.

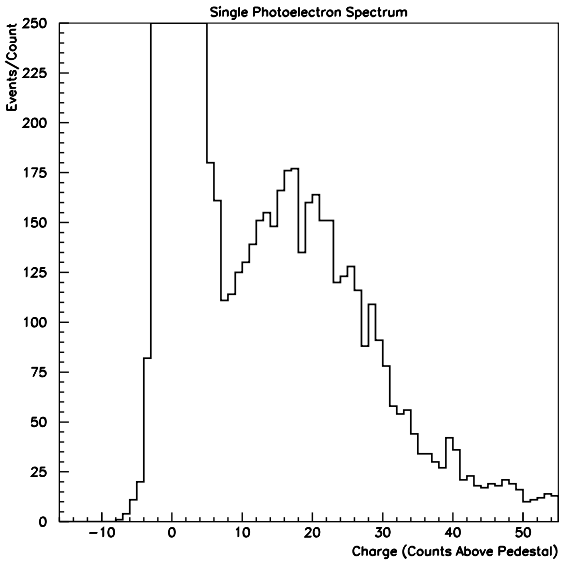

Fig. 10. Single photoelectron spectrum using the full electronics chain with an *in situ* SNO PMT. The truncated noise peak reaches roughly 2000 counts.

7 Data Acquisition

In this section the design and functioning of the SNO Data Acquistion System (DAQ) is outlined. First, a general overview of the system architecture is presented, followed by a more in-depth discussion of the details of the readout and control, event-building, and low- and high-level monitoring software.

The principal hardware components of the SNO DAQ system are a single VME crate containing a Motorola 68040 single-board computer without an operating system (the embedded CPU, or eCPU), but with 32 MByte of on-board memory. A PCIbus-VME interface (the Macintosh Dual-Port Memory or MDPM) with 8 MByte of memory, an SBus-VME interface (the Sun Dual-Port Memory or SDPM) with 8 MByte of memory, the Master Trigger Card (MTC), and the seven XL1 cards needed to access the 19 "SNO crates" containing the front-end electronics also reside in this crate.

Each SNO crate is read out sequentially by the eCPU, which accesses one crate in turn through the transparent XL1/XL2 interface bus. Within each crate, the FECs are read out sequentially, by programming the slot-select register on the crate's XL2 card.

Once the contents of the FEC memory have been read by the eCPU, they are transferred to a circular buffer on the SDPM. The eCPU additionally has access to the Master Trigger Card memory; once it has checked every enabled FEC, it reads out the MTC memory and transfers the trigger data to a separate circular buffer on the SDPM.

The SDPM is simultaneously and asynchronously accessed in read-only mode by a Sun Ultra Sparc 1/170 workstation, which is responsible for sorting the FEC and MTC data and building them into events. The Sun writes full events to disk. A separate mechanism is responsible for copying completed event files to a tape drive located on this Sun as well as copying, via Ethernet, these files to a Sun on the surface, where they are copied again to tape. The system also supports monitoring programs running on a variety of platforms. These monitoring programs access a sampled data stream in real time over the network.

The readout of the electronics is both controlled and monitored via a user interface Program, the "SNO Hardware Acquisition and Readout Control (SHARC)," running on a Power Computing 250 MHz PPC Macintosh compatible, which uses the MDPM to communicate with the eCPU. A set of small, predefined data blocks transfer control and low-level monitoring information such as user commands and eCPU status between SHARC and the eCPU. SHARC initializes the hardware, takes individual hardware elements (channels, cards, crates) in and out of the readout, stores the current hardware

configuration (which elements are present and which are being read out), and ensures that this information is saved.

SHARC controls SNO's calibration sources through a manipulator computer that moves the sources around inside the detector, and also receives information regarding individual source status from the various computers used to operate the different sources themselves. The manipulator or "calibration" computer inserts this slowly-varying data into the data stream by sending it to SHARC, which writes it to a calibration data block in the MDPM. Source information that changes more quickly (additional trigger information, more precise timing) is generated if necessary by routing the relevant signals from the sources to spare FECs and integrating the resulting data into the data stream exactly as if it were coming from the PMTs. Interpretation of the data is left to the offline analysis.

The eCPU reads the current configuration from a control block in the MDPM that has been loaded by SHARC during initialization. It loops over the desired hardware, incrementing error registers in the MDPM if read or write errors are detected, and attaching information identifying the bad crate or card. The eCPU periodically checks the configuration block for changes, which if detected will alter the readout loop. In this manner, individual cards or even entire SNO crates can be removed from the readout loop. A MDPM-resident control structure containing "start" and "stop" semaphores is also polled periodically, and enables global control of the readout.

Removing hardware from the readout loop or pausing the readout entirely does not prevent data from being stored in the FEC memory. Each FEC holds up to $\sim 350,000$ PMT hits, several hours of data under normal detector operation. Individual channels (bad PMTs) are taken offline through software by writing to a FEC register that prevents the channel data from going into the FEC memory.

The eCPU transfers the FEC and MTC memory contents to two circular buffers in the SDPM, 7 and 1 MByte in size, respectively. The eCPU updates a buffer write pointer, while the Sun updates a buffer read pointer, enabling the eCPU to track the Sun's readout progress. The eCPU will pause the readout of the hardware if either buffer fills up and will wait until the Sun catches up.

Whenever it is changed, a copy of the configuration control block is written to a block in the SDPM by the eCPU, where it is read by the Sun and incorporated into the event data stream.

The Sun, once it has read out the SDPM, sorts through the MTC and FEC data and aggregates PMT hits plus MTC trigger information into events. Events are stored in a buffer for some period of time to ensure that any late PMT hits can still be associated with the proper event. Once the latency period

expires, the events are passed to a FORTRAN process, which translates the data into ZEBRA format [28] for use by the offline analysis and writes the resulting files to disk.

In order to monitor the state of the eCPU code, the MDPM control block contains, in addition to the start-stop semaphores, a pair of "heartbeats," counters that are incremented in turn when the eCPU is looping over the readout, or in a tight loop waiting for the start semaphore to be set. The user interface for SHARC displays these heartbeats.

Data from the Sun, either in raw, pre-event-built form or as completed events, are transmitted over the network to a Sun resident process, called the Dispatcher, which rebroadcasts the data to any clients requesting it. As this rebroadcast is also over the network, clients can be located anywhere. The Dispatcher also receives data regarding run conditions from the control Mac. The data are labelled, and different clients can request data with different labels. Clients receive only as much data as they can process, and any data unsent by the Dispatcher is overwritten after some time. For high-rate data, *e.g.,* certain types of calibrations, the monitor system behaves as a sampling system. The system is extremely modular, and clients on various platforms can connect and disconnect from the Dispatcher at will. Because of this separation between the Dispatcher and the monitors, the Dispatcher itself is very stable.

Tools available for both UNIX and Mac platforms allow one to examine the raw PMT data, MTC data, or full event data, to check for data integrity, and to examine data either on a crate-by-crate basis or for the full complement of channels. There are several tools for event display in the SNO detector geometry. In addition, there are Web-based monitoring tools that update HTML files on a designated server for displaying more static information of interest to the offsite collaborator.

8 Neutral Current Detector Array

The detection of a free neutron is the signal that a neutral-current (NC) event has occurred, while the detection of a neutron (or two neutrons) in coincidence with a positron indicates a $\overline{\nu}_e$ interaction. Heavy water is an excellent moderator, and a number of possible strategies for detecting neutrons can be devised. One such strategy, discussed in Sections 1 and 2, involves the addition of a chloride salt to the D_2O. When a neutron captures on 75% abundant ^{35}Cl, it emits 8.6 MeV in γ rays, which mainly Compton scatter. The resulting Čerenkov radiation emitted by the electron can be detected by the PMT array in the same way CC events are detected, and the Čerenkov-light patterns

produced by γ rays distinguished from those of electrons on the basis of their greater isotropy.

Alternatively, neutrons can be detected with high efficiency in ^{3}He-filled proportional counters. An array of such counters, with a total length of 770 m, and constructed of highly purified materials, has been designed for SNO [29]. In this way, the NC and CC events can be recorded separately and distinguished on an event-by-event basis. Event-by-event sorting makes optimum use of available statistics, and simplifies interpretation of sparse signals, such as from a distant supernova.

Detection of thermal neutrons by the reaction

$$^3\mathrm{He} + \mathrm{n} \rightarrow \mathrm{p} + {}^3\mathrm{H} + 764 \text{ keV}$$

takes advantage of an enormous cross section, 5330 b, and is a well developed art that has included applications in neutrino physics [30–32]. Nonetheless, the design of an array of ^{3}He proportional counters for SNO poses unusual problems.

The neutron production rate in SNO is expected to fall in the range 6 to 42 neutrons per day based on the measurements by the SuperKamiokande Collaboration [33] of the rate of ν-e scattering, but not the flavor composition. The rate predicted by recent solar-model calculations [6] is 13 per day when the cross-section calculated by Kubodera and Nozawa [34] is used. The neutron signal must not be overwhelmed by backgrounds from naturally occurring radioactivity in construction materials, nor can substances be allowed to leach significantly into the heavy water and interfere with water purification. Helium permeates readily through many otherwise acceptable materials. The counters are to survive under water at absolute pressures up to 3.1 atm for ten years or more, placing stringent demands on detector longevity and stability. A counter array with high neutron efficiency is needed, but not at the cost of significantly obscuring the Čerenkov light from CC events. These conditions severely constrain detector design, the materials employed in constructing the detector array, and the methods of handling and deployment.

Backgrounds of several kinds can be present. Most serious is photodisintegration of deuterium by gammas above 2.22 MeV, as the neutrons produced are indistinguishable from the ν-induced signal.

At the bottom of the natural Th and U decay chains are two sufficiently energetic gammas. Many cosmogenic activities also have high energy gammas, but only one, 78-d ^{56}Co, has a long enough half-life to be relevant. Energetic photons can also be produced by capture of neutrons and by $(\alpha,\mathrm{p}\gamma)$ and $(\alpha,\mathrm{n}\gamma)$ reactions.

Table 4
Capture percentages of neutrons by isotope, for pure D_2O and for pure D_2O with NCDs installed.

	Pure D_2O	NCDs
^{3}He		36.6
Ni		1.6
D_2O	66.9	36.9
H in D_2O	16.5	9.1
D in D_2O	32.0	17.7
O(n,γ) in D_2O	5.8	3.2
O(n,α) in D_2O	12.6	6.9
Acrylic	28.4	20.9
H_2O exterior to AV	4.7	4.0

Alpha particles emerging from the wall of the proportional counter can leave the same amount of ionization in the gas as a ^{3}He(n,p)T event, as can electrons from β decay and Compton scattering. Even very low-energy events, such as the decay of tritium, can compromise the signal via random summing.

The principal defense against these backgrounds is to minimize radioactivity in construction materials and to assure a high degree of cleanliness during assembly. To supplement those measures, techniques for pulse-shape discrimination and position encoding are used, both of which require digitizing the pulse ion-current profiles event by event. Spurious pulses from high-voltage breakdown and electromagnetic interference must be controlled. Backgrounds of all types must not only be minimized, but in addition there must be robust techniques to measure them *in situ*.

Because of the efficiency of heavy water as a neutron moderator and the high cross-section for neutron capture on ^{3}He a rather sparse array of neutral-current detectors (NCD) is sufficient. An array of 5.08 cm diameter proportional counters with a total length of 770 m arranged on a square lattice with 1 m spacing gives a neutron capture efficiency of approximately 37% (see Table 4) with tolerable interference to Čerenkov light produced via the charged current interaction. Approximately 15% of uniformly generated optical photons are absorbed.

At modest pressures of 1-3 atm of ^{3}He, the counters are essentially "black" to thermal neutrons. For 99.85% enriched heavy water, the mean distance from the point of generation to the point of capture for thermal neutrons is calculated to be 110 cm and the mean time to capture 16 ms with the NCD

array, compared with 48 cm and 4 ms, respectively, for 0.2% $MgCl_2$.

The detectors are filled with a gas mixture of 85% ^{3}He and 15% CF_4 at a total pressure of 2.5 atm to provide a good compromise between gas gain and stopping power (to mitigate a "wall effect" wherein either the proton or the triton strikes the wall before the end of its range). A lower pressure, and therefore operating voltage, would simplify microdischarge management and increase drift speeds, but would require thick-walled counters to resist collapse. At the bottom of the SNO vessel, the absolute pressure is that of a column of D_2O of height 16.8 m plus 1.3 atm of air pressure, for a total of 3.1 atm.

The copper anode wire of diameter 50 μm is low in radioactivity and ohmic losses. At 1650 V the gas gain is approximately 100. For higher gas gains positive-ion space charge at the wire causes the avalanche multiplication to depend increasingly on track orientation.

Trace amounts of electronegative contaminants such as oxygen and water degrade severely the performance of the gas in a sealed counter. Consequently, counter surfaces are electropolished, acid-etched, baked under vacuum, and purged with boiloff N_2 prior to fill. The chemical treatment also removes surface debris stripped off the mandrel during the fabrication process.

The ^{3}He gas from the Department of Energy facility in Savannah River contains a small amount of tritium, about 0.5 mCi/l, which is reduced to 5 nCi/l or less by passage through a charcoal-loaded cold trap and by recirculation through a SAES, Inc., St101 getter. At that level, random coincidences and pileup of tritium decay pulses are no longer a concern in the energy regime of interest. Some detectors, about 5% of the total by length, are filled with ^{4}He:CF_4 to provide a check on backgrounds.

The NCDs are fabricated in three different unit lengths in order to fill the sphere efficiently. (An upper limit is set by the dimensions of the cage in the INCO Number 9 shaft, which permits an object 3.7 m long to be brought down.) The active length is 13 cm less than the mechanical length. Fig. 11 shows the main features. The important mechanical parameters of the detectors are summarized in Table 5.

The bodies of the proportional counters are made of ultrapure nickel tubes fabricated at Mirotech (Toronto) Inc., by thermolysis of $Ni(CO)_4$ vapor at the surface of an anodized aluminum mandrel heated to 215 C. A limited number of elements (Pb, Ra, Th, and U not among them) react with CO to form carbonyls, and the metals formed by chemical vapor deposition (CVD) from this precursor can be expected to be free of the most troublesome radioisotopes. The nickel deposit has properties very similar to conventional metallurgical products. Radiochemical neutron activation analysis has shown Th levels in the bulk material of order 10^{-12} (1 ppt) by weight or less.

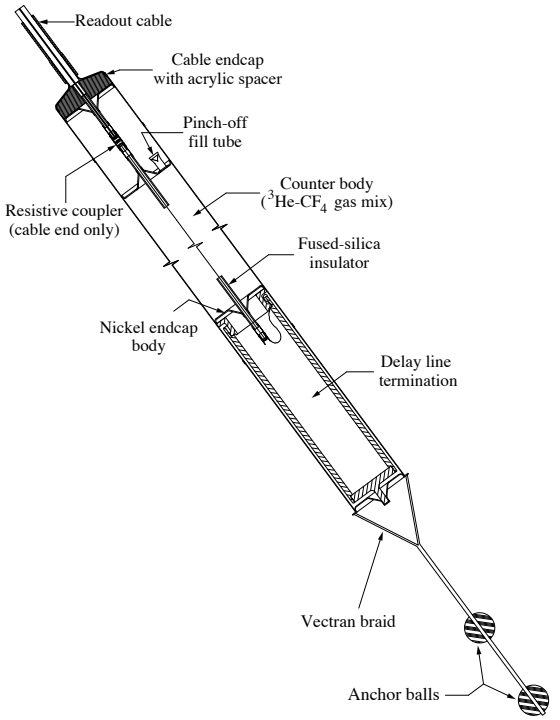

Fig. 11. SNO neutral-current detector.

Nickel is a relatively inert metal. The exposed macroscopic surface area in SNO is 125 m^2. In 17.3 MΩ-cm water the measured leach rate is $\leq$22 μg m^{-2}d^{-1}, which is not expected to compromise the operation of the water purification plant.

Endcaps are also made by CVD, in this case on stainless steel mandrels, and are welded into the tubes with a Lumonics 50-W Nd-YAG laser welder. Insulators are Heraeus-Amersil Suprasil T-21 synthetic fused-silica tubes. The insulators are internally coated with a layer of pyrolytic graphite at anode potential to eliminate electric fields inside them. They extend 2.5 cm into the gas volume to act as field tubes and prevent multiplication of electrons from regions where the electric field is distorted. A silica-nickel seal is highly

Table 5
Important physical parameters of the NCD detectors.

Item	Value	Variation	Units
Wall thickness	0.036	$^{+0.012}_{-0.000}$	cm
Length	200, 250, and 300		cm
Diameter	5.08		cm
Wire diameter	50		μm
Gas pressure	2.50	$\pm$0.03	atm
Weight	510		gm/m

mismatched, so the design places the silica under compressive stress at working temperatures to take advantage of the high compressive strength of that material. Techniques were developed in collaboration with IJ Research (Santa Ana), Inc. to metallize the seals and solder them with a 96.5:3.5 eutectic Sn:Ag alloy. Counters are filled through copper tubes, which are then pinched off. All assembly is carried out in a Class 1000 cleanroom.

The individual units are welded together at the time of deployment in SNO in 96 "strings" of length ranging from 4 m to 11 m. A total mechanical length of 770 m is to be deployed in the heavy water. The strings are installed by a remotely operated vehicle (ROV) once the vessel is filled with heavy water. Each string is anchored to an attachment point affixed to the bottom of the acrylic vessel and floats upward, restrained by a flexible braided anchor cord made of Vectran fiber.

Spaces of 35 to 50 cm are left between the string ends and the vessel. The bottom of each string is terminated with a 30 ns open-ended 415Ω delay line to facilitate position readout by pulse-reflection timing. A single 91Ω coaxial cable, made of copper and polyethylene by South Bay Cable (Idyllwyld, CA), Inc., carries signals from the top of each string up the neck of the vessel to preamplifiers. The cable specific gravity is 0.955.

In Table 6 are listed some of the decay properties of relevant isotopes. Since detection of Čerenkov light is the principal means of quantifying the photodisintegration background *in situ*, the production of light by other activities is also important.

By means of a suite of radioassay techniques (neutron activation analysis, radiochemical methods, direct gamma counting, alpha counting) applied to samples and to the complete inventory of smaller components, quantitative predictions can be made concerning the levels of photodisintegration and other backgrounds that will accompany the NCD array in SNO. A neutron production rate of 100 per year in the SNO vessel results from 1.1 μg of Th

Table 6
Photodisintegration and high-energy beta emitters.

Isotope	$E_{\beta(max)}$, MeV	E_γ, MeV	γ branch, %	(γ,n) Probability
^{212}Bi($\rightarrow^{208}$Tl)	1.8 (18%)	2.615	36%	1/470 (per γ)
^{214}Bi	3.26 (18%)	2.445	1.5%	1/750 (per γ)
^{56}Co	1.8	var.	-	1/1125 (per decay)
^{228}Ac	2.06 (11%)	var.	89%	0
^{234m}Pa	2.28 (100%)	-	-	0
^{40}K	1.3 (89%)	1.46 (EC)	11%	0

in equilibrium, or 12.8 μg of U in equilibrium. Slightly more than half of all neutron-capture events can be unambiguously identified via track length *vs* energy as being distinct from alpha particles (for this reason the array efficiency is taken to be 25% rather than the nominal 45% capture efficiency). Electron and Compton backgrounds, and microdischarge events, have topologies separated still further from neutron events. As a result, photodisintegration is the only background requiring a separate determination and subtraction, which can be accomplished by measurement of the Čerenkov light emitted by radioactivity. Assays still in progress preliminarily indicate that the NCD array will contribute fewer than 300 neutrons per year.

9 Control–Monitor–Alarm (CMA) System

The Control–Monitor–Alarm (CMA) system is the data-acquisition and control system for the underground laboratory environment. The system monitors approximately 250 analog and 220 digital readings. Major functions of the CMA system are:

- Hazardous gas detection;
- Environment monitoring (temperature, humidity, air pressure);
- Cooling and air-circulation control;
- Load and position sensing on critical structural elements;
- Electrical system monitoring;
- Control of the magnetic compensation coils for reduction of the effect of the earth's field;
- Monitoring of supply voltages and currents for the electronics;
- Logging of various monitored parameters.

The system uses Paragon TNT industrial automation software from Nemasoft [35]. The hardware was furnished as a complete system by Sciemetric In-

struments [36]. Analog readings are converted by a single multiplexed 20 kHz 12-bit ADC. Voltages up to ±10 VDC can be converted in seven software selected ranges. Industrial 4–20 mA signals are converted to voltages with precision resistors. Digital inputs may be 24 VDC or 120 VAC. There are 32 solid-state relay channels for digital output. The input/output scan rate is up to 2 Hz. Systems with independent microprocessors (such as the cooling unit, and the uninterruptable power supply) have serial links for ASCII output to the CMA.

The CMA software is presently running on a dual 200 MHz Pentium-Pro system with 256 MBytes of RAM running Windows NT 4.0. Remote systems running Paragon TNT software can connect via TCP/IP with the underground system. A remote monitoring system is kept running in the SNO surface building. Critical alarms are annunciated on the surface as well as underground.

Data are recorded continuously in a Microsoft Access database on the main CMA system, and are exported periodically to the custom SNO database. The data logging program enters a new record only when a significant change in a parameter has occurred.

10 Calibration

Accurate measurement of the physics processes in the SNO detector requires a chain of calibrations and calculations to connect the raw measured quantities of PMT charge and time to a full description of the interaction in terms of energy, direction, and particle type. This set of calibrations includes built-in electronic calibrations, several dedicated optical calibrators, various types of tagged and untagged radioactive sources and detailed radioassays of the detector materials. Taken together with a comprehensive Monte Carlo simulation of the detector, this set of calibrations creates an overdetermined model of the detector that can be used to interpolate energy scales and particle identification across the full response range of the detector. The major calibration tools are listed in Table 7 and briefly described in the following sections.

The conversion of the digitized values for PMT charge and time to photoelectrons (pe) and nanoseconds (ns) is a two-step process, involving electronic pulses and light flashes from known positions within the detector. The electronic pulser calibration yields the transfer functions and offsets (pedestals). The establishment of a common time reference for all channels (t_0) is performed with optical sources.

The charge offsets (pedestals) are the values digitized when there is no charge input from the PMT. The time offset is found using a full time ramp. During calibration, each cell (there are 16 analog memory cells per channel for each of the three charge and one time measurement) is given 10 event trigger pulses without any PMT input. Because the pedestal calibration is done during normal running there are occasional coincidences with noise or detected light that must be removed during the analysis stage. In the offline analysis, two passes are made through the data. The first pass determines the value of the digitization that occurs most frequently, and then events that are more than ±10 units away from this peak digitized value are discarded for a second pass that determines the mean (pedestal) and RMS for each cell. Should more than a certain number of events be rejected with this cut, the cell is flagged and not used again until recalibration or repair. The RMS is typically less than one ADC count and cells with an RMS greater than three counts are flagged. The pedestals are run constantly in background while solar-neutrino data are being taken.

Table 7
Calibration devices for the SNO detector and their principal uses.

Device	Calibrations
Electronic Pulsers	Time slope (ns per count); Time pedestal; Charge slope (pC per count); Charge pedestal
Laser Ball; Sonoluminescent Source; LED Sources	Common time reference (t_0); D_2O absorption and scattering (λ); Acrylic absorption and scattering (λ,r,θ); H_2O absorption and scattering (λ); Reflection and scattering from structures; Single photoelectron (pe) response ; Relative single pe efficiency; Multiple photoelectron response; Walk (time vs. pulse amplitude)
Radioactive Sources: ^{16}N, ^{252}Cf, ^{8}Li, Th, U	Gamma energy response; Electron energy response; Neutron-capture efficiency; Angular response
^{3}H(p,γ)^{3}He Accelerator Source	Gamma energy response
Tagged Sources: ^{252}Cf, ^{24}Na, ^{228}Th	Gamma energy response; Neutron-capture efficiency
Radioassay	Backgrounds from construction materials; Backgrounds from water contaminants

Individual voltage pulses of varying width and amplitude (and, thus, charge) are fed to the PMT inputs to measure the high gain, long integration (QHL), high gain, short integration (QHS), and low gain, selectable integration (QLx) signals. Each cell is pulsed ten times for a given injected charge (Q_{inj}). The charge injection is incremented in steps up to a maximum value. A low-order polynomial fit of digitized value vs. Q_{inj} is performed for each cell offline.

The time calibration sends one pulse to the PMT input and a delayed pulse to the event trigger; the time difference between the pulses is varied by a known amount in steps as small as 100 ps. The slope calibration procedure is similar to that of the charge calibration. The relation between the time digitized value and nanoseconds between two generated pulses is monotonic over most of the range.

The risetime of the PMT pulses and leading-edge discrimination lead to a timing dependence on the PMT anode charge. Calibration of this effect is made by running the laserball at various intensities from a fraction of a pe per PMT to hundreds of pe per PMT, and then creating charge versus time (QvT) histograms for each PMT.

Because many of the optical- and particle-calibration techniques are position dependent, a general-purpose manipulator has been developed to provide source deployment at accurately known off-axis positions in two orthogonal planes in the D_2O. (In addition, six calibration access tubes run from the deck to positions in the light water.) The source manipulator is a carriage located in a plane by two Vectran ropes (see fig. 12) that run down the vessel neck through pulleys on the carriage to fixed locations on the acrylic vessel. A third, center rope connects directly to the source carriage. The source can be introduced at the neck and visit 70% of the plane with a position accuracy of better than 5 cm.

At the deck interface the carriage is pulled up into a glove box that is part of the cover-gas volume. There a person can work on a source while keeping the detector isolated from light and airborne radioactivity. The source can then be pulled through a gate valve into an interlock box where it can be removed or serviced.

Some of the calibration sources require power cable, signal cable and/or gas capillary connections to equipment on deck. To provide uniform and reliable manipulator operation, these auxiliaries are cabled into a standard sized umbilical cable. The umbilical cable runs through the center of the source carriage to a compression fitting at the top of the source. The cable connections are then internal to the source. The umbilical cables are stored and paid out from a pulley array mechanism held under tension, thereby avoiding twisting of the umbilical cable.

Optical sources are used in both the optical calibration and the electronics calibration. They include a wavelength-selectable dye laser, a sonoluminescent source, and light-emitting diodes (LEDs). Both the laser and sonoluminescent source have emission times well suited to making precision timing calibrations. The LED sources are slightly broader in time, but multiple sources in well-surveyed positions offer a useful and easily operated check on the detector

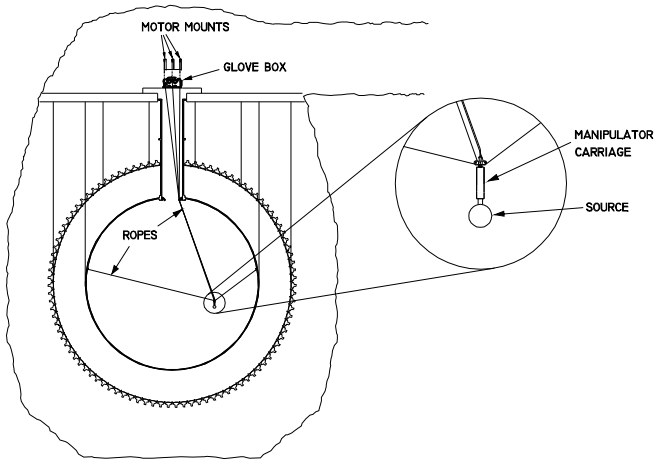

Fig. 12. SNO calibration source manipulator system.

geometry and stability.

The nitrogen or dye laser with a fiber-optic cable to a diffuser ball ("laserball") is the primary light source [37]. The laser (Laser Photonics Inc. LN203C) provides pulsed radiation at 337.1 nm with a 600 ps pulse width and peak power of 150 kW. The laser pulses up to 45 Hz and can be used directly or as a pump for several dye lasers that provide wavelengths in the range of 360–700 nm. Neutral-density filters mounted into two selector wheels allow remote intensity adjustment. The laser light is delivered to a diffuser ball via a fiber-optic bundle within an umbilical cable.

The dye laser frequency and attenuation filters can be adjusted remotely by computer control. The output from the dye lasers is focused into quartz fiber with length 1 m and diameter 1 mm (Fiberguide Ind. SFS-1000N) to enhance beam structure stability.

The laser pulses are transmitted to the detector by a bundle of 22 high-OH 100 μm silica step-index fibers (Fiberguide Ind. SFS-100/110/240/310N). These fibers offered the best combination of UV transmission, low dispersion and cost. The fiber-optic umbilical cable terminates with a 10 cm diameter diffuser ball that serves to distribute light quasi-isotropically through the detector. A plug at the neck of the ball contains a fiber-optic positioning guide

tube and also houses a miniature monitoring PMT (Hamamatsu R5600). The fiber-optic guide tube allows the umbilical cable to be detached from the laserball and reconnected with no effect on the light output pattern. The light distribution pattern from the laserball is mapped out with monitor PMTs by rotating the ball in a dark room. The diffuser ball light pulse width is about 2 nsec (FWHM).

A sonoluminescent source provides bright, isotropic light of extremely short duration. Single bubble sonoluminescence (SBSL) can occur when an air bubble is introduced into water at the node of an intense, spherically symmetric sound field. The light[38] has a very short (< 100 ps) pulse width and a frequency distribution corresponding to a blackbody at a temperature of over 20,000 K [39], very similar to the Čerenkov spectrum. The relatively high repetition rate ($\sim$25 kHz) offers a good test of the system's burst capability. The short pulse width and isotropic output make the SBSL source useful for PMT timing calibrations and some optical analysis. In addition, the SNO detector provided an opportunity to investigate a variety of fundamental properties of SBSL [40].

The SNO SBSL source consists of a 250 ml spherical flask with two cylindrical piezoelectric transducers. The flask is housed within a sphere made of two 15 cm radius hemispherical acrylic sections to provide an air buffer. It is filled with pure distilled water to the neck level, and driven at the natural monopole resonance (28.5 kHz) with an inductively matched circuit. A small microphone transducer aids in scanning the frequency to find the natural resonance.

A bubble is generated remotely with a nichrome heater wire within the water. The bubble stability is monitored by observing the spikes on the microphone voltage trace. As sonoluminescence output begins, the light output is monitored with a small PMT (Hamamatsu R5600) within the acrylic source housing. The light output contains of order a million blue photons which are isotropically distributed in space when averaged over time scales of seconds or longer. The heater wire also provides some control over the light intensity, which decreases with increasing water temperature.

Light emitting diodes provide a simple and robust optical source for verification of water transparency, acrylic vessel and source positions, and PMT response. During the final construction stages of the PSUP, new LED products became available from Nichia Corporation. These indium-gallium nitride single quantum well (NSPB500) and double hetero-structure (NLPB500) devices offer high intensity blue radiation (420–480 nm), and the latter device can even emit in the UV (380 nm) when strongly overdriven in pulse mode [41]. A pulse of width approximately 7 ns is observed. Six of these devices have been packaged with a pulser circuit and mounted at the locations, in cm, (695, 248, 399), (-162, 681, -463), (-699, 49, -462), (-8, -764, -346), (698, 54, -463), and

(37, 1, -838) on the PSUP, where the center of the PSUP is (0,0,0), the z axis is up, and the x and y axes are defined with respect to construction coordinates.

The optical calibration process results in the determination of attenuation and scattering coefficients for the heavy water, light water, and acrylic [45]. By using the various measured optical coefficients, it is possible to simulate via a Monte Carlo calculation the optical transport of Čerenkov light produced by a neutrino or background particle. These simulations can then be used to interpolate (in space and amplitude) between the various energy calibrations discussed in the next session.

Most of the optical analysis is performed using data from the quasi-isotropic laserball at near single photoelectron (spe) light intensity, and utilizes the detected light intensities as a function of the calibrated time between the fast laser trigger and the digitized time value of the PMT discriminators. Light reflected from various parts of the detector produces substructure in the time distribution. This substructure can be used to characterize the optical properties of various parts of the detector, such as the PMT reflectors and the acrylic vessel, and to determine the Rayleigh, Mie and large particulate contributions to the scattering of light in the water volumes [46,47].

By moving the laserball to various off-center positions, absorption coefficients can be measured. Calibration source access ports into the H_2O volume within the PSUP will aid in determining the light attenuation in the acrylic panels. The relative PMT anode efficiencies and the overall optical "gain" of the detector are to be monitored at the spe level over time, and can be separated from changes in other optical constants by taking data at several source positions and at 400 nm where the acrylic transmission is high and uniform across acrylic sheets.

There are three gas transport sources: a ^{16}N gamma ray source, a ^{17}N neutron source and a ^{8}Li beta source [42], of which the ^{16}N is fully developed. The gas transport sources consist of a D-T generator neutron source, a neutron target chamber, gas capillaries, and decay chambers that can be deployed within the detector. The D-T generator, producing 14 MeV neutrons, is enclosed in concrete 30 m from the detector. Various target chambers can be moved into the neutron flux by stepper-motor control. Gases from the target chamber are routed via capillaries to the deck area and down into the source umbilical cables. The decay chambers can attach to the manipulator carriage and connect to the umbilical cable gas lines.

The ^{16}N is produced via (n,p) on the oxygen in CO_2 gas and decays by a beta delayed 6.13-MeV (66%) or 7.12-MeV (4.8%) gamma ray with 7.13-s half-life. The decay chamber is 41.9 cm long and 5.7 cm radius, and is made from 5-mm thick stainless steel so that the electrons (which have a 10-MeV endpoint

energy) are absorbed. A beta tag is provided by a 3-mm thick scintillator sleeve on the inside of the chamber with a 5-cm PMT. The source has been tested in the SNO detector and produced over 300 ^{16}N decays per second.

To reach gamma energies above 6 MeV a miniature accelerator source drives the ^{3}H(p,γ)^{4}He reaction to produce 19.8 MeV gammas [43]. The source consists of a cold-cathode Penning ion source, electron optics for beam extraction and acceleration, and a fixed target. It is housed in a 25-cm diameter, 60-cm long stainless steel capsule and operates with a beam voltage of 20–30 kV to produce approximately one photon per second.

Tagged sources have been developed that permit specific kinds of events in SNO to be identified by time coincidence with a trigger, allowing one to acquire calibration data in an essentially background-free manner. Such sources are valuable for testing PMT response, particularly at low energies, for determining backgrounds, for checking neutron transport simulation code, and for calibrating event reconstruction.

Tagged neutron sources are fabricated using ^{252}Cf at several different activity levels. The 2.64-y ^{252}Cf decays with a spontaneous fission branch at 3.09%, which provides neutrons and a trigger from fragment betas and gammas.

Another tagged source is constructed from a NaI crystal coupled to a PMT. The crystal is activated to produce 15-h ^{24}Na. The trigger can be gated on the energy deposited in the NaI in order to tag the 1.37 MeV or the 2.75 MeV gammas in SNO to study the response to low-energy gammas, and to measure photodisintegration neutrons. A third source [44] under development is a polycarbonate-housed proportional counter with a radioactive source (*e.g.*, ^{228}Th) deposited on the anode wire. The source is designed so that emitted betas will deposit little energy in the counter and will mimic the spectrum produced by natural radioactivity present in SNO.

After correcting for relative response due to position and direction, an event is assigned an energy according to a calibrated NHIT scale. The ^{16}N source sets the absolute scale and provides a measurement of the energy resolution for a 6.13-MeV gamma ray. The energy response to electrons will be inferred from this measurement since the difference in response between gamma rays and electrons is well modeled with the EGS4 code and will not contribute significantly to the uncertainty in the electron energy scale. For each event there is a significant probability for recording unrelated noise hits. The rate of background hits is directly measured by regularly sampling the detector using the pulsed–GT trigger. The high-energy end of the scale is calibrated with the accelerator source.

The detector angular resolution is primarily determined from theoretical treatment of electron scattering and production of Čerenkov light, together with

the geometry of the PMT array. The treatment can be verified through the Monte Carlo against data from the ^{16}N gamma source. If the fitted event position is taken to be the point of momentum transfer from the gamma ray to the electron, then the initial direction of electron motion for single Compton interactions is the vector to this position from the ^{16}N source position. A cut on large radial distances reduces the source angle uncertainty, while a cut on the larger NHIT events will select mostly those events of large momentum transfers to the electron in the first scatter. Deconvolution of the Compton scattering angle can be accomplished with the Monte Carlo simulation.

11 Control of Radioactive Contaminants

The minimization of background events requires a high intrinsic purity of materials and the reduction of radioactivity on the surfaces of the detector components. The purity of materials was addressed at the time they were selected for fabrication by measuring the activity in samples. Low background $\gamma-$ray counting and neutron activation analysis have been used extensively for analysis of different materials in the SNO detector. Since the detector is located in an active mine where the rock and ore dust contains typically 60 mg/g Fe, about 1.1 μg/g U, and about 6.4 μg/g Th, while the inner components of the detector require at or below 10^{-12} g/g U and Th, dust levels had to be kept very low. A program to keep contamination as low as reasonably achievable during the construction and operation of the detector was planned from the inception of the experiment. This section describes the methods for controlling and reducing surface contamination.

Radon (^{222}Rn) is of special concern in the SNO detector, since it can diffuse from components, dust or the cavity walls into the water and move into critical regions of the detector. Radon emanation from components depends on diffusion properties as well as the U content, and hence it varies with the density, hardness and surface properties of the materials. Extensive measurements of radon emanation were carried out in both vacuum and water test chambers for all critical materials for the SNO detector.

Because of the presence of small amounts of radioactive contaminants–1.1 ± 0.2 μg/g U and 5.5 ± 0.5 μg/g Th in the host rock and 1.2 ± 0.1 μg/g U amd 2.4 ± 0.2 μg/g Th in the concrete liner–in the SNO detector cavity, radon ingress from the cavity walls is a potentially serious background source. Radon diffusion studies were carried out on several polyurethane coating materials, both in the laboratory and in an underground test facility, to determine the radon attenuation properties of these sprayed-on coatings. To meet the design maximum of 12 radon atoms per square meter per hour diffusing into the cavity from rock, concrete and liner materials, the coating material (Ury-

lon HH453 and 201-25 polyurethanes) was required to be 8 ± 1 mm thick. The coating was applied to a smooth concrete base on the cavity walls and floor in 9 separate layers (of alternating white and gray colour). The coating thickness was monitored with a portable probe, developed especially for this work, which measured the amount of backscattered x-rays from a radioisotope source mounted in the probe [48]. This backscatter signal was proportional to the coating thickness and a standard calibration procedure was developed to give coating thicknesses directly. The coating is expected to attenuate radon from the walls by a blocking factor of 2×10^{-7}.

Contamination control at SNO has several elements. At the beginning of assembly of the detector a clean environment (air and surfaces) was established in the underground laboratory and maintained throughout construction. The entire laboratory became, and continues to be, a clean room. Fresh air entering the laboratory and the air that is cooled and circulated within much of the laboratory passes through HEPA filters. Detector components were cleaned above ground and appropriately packaged for shipment underground. Material and equipment enter the laboratory through an interlocked area with high-pressure water cleaning equipment. Personnel take wet showers and put on clean garments before entering the laboratory proper. These transition areas, the car wash and the personnel entry, are indicated on the general layout of the laboratory (see Fig. 1).

The surfaces of the laboratory (walls, floors, and construction equipment) were cleaned repeatedly as necessary during construction. Personnel pass through air showers at critical locations. Components of the detector (such as the acrylic vessel) were given a final cleaning after assembly. Components that could not be accessed for cleaning or that have topologically complicated surfaces, for example, the PMTs and reflectors, were covered wherever possible with clean tarpaulins or plastic sheeting (dust covers), which were removed at a later time. Dust covers were used extensively in the construction of the acrylic vessel and the PSUP. Toward the end of construction, the infrastructure (platforms, ladder ways, ductwork, elevator, etc.) was removed in a manner that left the detector cavity clean. Care was required as much of this infrastructure was installed before the cavity was first cleaned.

At the end of construction the cavity deck was sealed to inhibit the movement of radon, and a separate clean room was established on the deck above the chimney of the acrylic vessel. This local clean room encloses the insertion points and devices that are used in the calibration and operation of the detector and subsequently in the installation of the neutral-current detectors.

To control surface contamination one must be able to measure it and to monitor the factors affecting it. Commercial air-particle counters are used to sample the number and sizes of fine particles in the air. The number of particles larger

than 0.5 μm in diameter in 28 l of ambient air defines the "class" of the air and of the clean room. Class values vary dramatically depending on the work going on in a particular area. In general, the quality of the air within the laboratory has been in the range of class 1000 to 10,000, depending on location and level of activity. The amount (mass) of dust that accumulates depends on the number versus size distribution and on the density of the particulate. Mass versus size distributions for mine dust were measured with a cascade impactor, and number-versus-size distributions with an optical microscope.

The dust deposition rate and the total accumulated dust are the most relevant quantities. Several methods were used to measure the amount of contamination on a surface. A quick method is the "white glove test," in which a white cloth, mounted on the sharp edge of an eraser, is wiped over a surface for a given distance. Through calibration measurements and adoption of consistent procedures this test has been made semi-quantitative, and it is sensitive down to about 0.5 μg/cm^2 of dust.

X-ray fluorescence spectrometry (XRF) was used for more sensitive and precise measurements. In this method, one detects elements in the range $Z = 20$ to 45 by the characteristic X-rays emitted following fluorescence of the sample with an x-ray tube. A spectrometer was built for this purpose and located underground for convenient use.

In one type of XRF measurement, thin, spectroscopically-pure plastic films were used as "witness plates" to collect dust over a known period of time. The amount of mine dust deposited was inferred by measuring the amount of iron, which is present in the local mine dust at the level of 7%. A sensitivity of about 0.1 μg/cm^2 is possible in a counting time of 20 minutes.

In a second type, dust is removed from a surface by placing a section of thin adhesive tape (low in Fe) on the surface, pulling it off and placing it in the spectrometer. When a single piece of tape is used to perform five lifts from adjacent areas on a surface, the sensitivity can be extended down to about 0.015 μg/cm^2. This method was used to monitor the surface cleanliness of the acrylic vessel.

A few direct measurements of U and Th in deposited dust were made using neutron-activation analysis to verify the correlation of Fe with U/Th.

During more than three years of construction since clean conditions were first established, fairly regular patterns and deposition rates emerged. The quality of the air was characterized by an average class value of 2500 ± 500. Average deposition rates ranged from 1 μg/cm^2/month of mine dust in busy areas to one tenth that amount in inactive areas. (The air particle counts and mass deposition rates are roughly consistent with the number-size distributions for airborne particulates measured inside the laboratory.) The level of cleanliness

on the surface of the acrylic vessel at the time of water fill was typically better than 0.1 μg/cm^2. (Zinc was also regularly observed in the XRF spectra at a level typically 20% of the mine dust. Zinc comes mainly from the use of galvanized scaffolding in construction.) Since a mass deposition of 1 μg/cm^2/month integrated over a thirty-month period would exceed the target contamination limits in any region of the detector, periodic cleaning of accessible surfaces and the use of dust covers on inaccessible areas was required to achieve target levels.

12 Offline Analysis and Simulation Code–SNOMAN

The offline software is required to perform two major functions: the analysis of SNO data, and a detailed and complete simulation by Monte Carlo techniques of all significant signals and backgrounds using as accurate a model of the detector and its response as possible. Both of these functions are combined in the SNO Monte Carlo and Analysis code, or SNOMAN. SNOMAN consists of a set of largely autonomous processors written primarily in FORTRAN. In order to ease distributed development and maintenance (and to overcome the lack of dynamic memory allocation in FORTRAN) these processors communicate through a central data structure managed by the CERNLIB package ZEBRA. ZEBRA is also the basis for the management of banks of data, called "titles." Titles-management routines in SNOMAN insure that as successive events are analysed the constants describing the detector response are the appropriate ones for that time and detector configuration. The use of autonomous processors working on a central data structure allowed staged development of the processors. Since at the time of this writing there are over 25 processors in SNOMAN, only selected ones will be discussed.

In addition to SNOMAN there is another major offline analysis tool: the SNO database, or SNODB, which is based on the CERNLIB package HEPDB. SNODB is a distributed master-slave database that runs collaboration wide via PERL installation and management scripts. The scripts set up SNODB on the large variety of platforms in use and manage the updates that keep the various slave copies of the database in step with the master copy. SNODB contains ZEBRA banks that encode all the information about calibrations and detector status, configuration, and performance which is needed to interpret SNO data.

The basic units of the data structure for the Monte Carlo are the vertex and the track. A vertex represents any event of interest in the movement of a particle (the origin of the particle, when it encounters a boundary, any interactions it undergoes, etc.), while tracks specify how particles move from one vertex to the next. The Monte Carlo can then be divided into generation (deciding

what seed vertices to create), propagation (taking the initial seed vertices and creating successive tracks and vertices based on the transport of that type of particle in the SNO detector, and creating any additional particle such as Čerenkov photons which the initial particle may spawn), detection (either of photons by the PMTs or of neutrons by the NCDs), and electronics simulation. In order to achieve accurate, usable code with the least time and effort well-established and tested software packages have been used wherever possible. For example the propagation of electrons, positrons, and gammas is handled by EGS4 [49] (modified to produce tracks and vertices), the propagation of neutrons is handled by routines lifted from MCNP [50], the muon physics is largely taken from GEANT [51], and much of the code that describes how the spectra might be modified by the MSW effect is taken from the work of Hata [52]. A large amount of work has gone into verifying several aspects of these modified external codes, which are particularly critical to SNO physics but which may not have been extensively tested in the past. In particular a considerable amount of effort has been expended on understanding the angular distribution of Čerenkov photons produced by an electron of a few MeV [53], which is important for some of the analysis techniques discussed below.

The Monte Carlo code for which reliable, pre-tested software like EGS4 was not available was written by the SNO collaboration. The photon propagation includes the effects of attenuation, refraction, reflection, and Rayleigh scattering (Mie scattering is expected to be negligible for the levels of cleanliness expected in SNO) as a function of wavelength and polarisation. The light concentrator/PMT response has been the focus of substantial software development and experimental effort. A detailed stand-alone simulation of a concentrator and PMT was written [54] and tested against experiment [55], then installed as a SNOMAN processor.

The geometry of the detector is a compromise between a totally data-driven system that would be slow but flexible and a completely hard-wired structure that would be fast but inflexible. The geometry consists of detector elements, each of which is made up of primitives (such as spheres, cylinders, elliptical toroids, etc.) for which the actual calculations are made. The ability to alter the complexity of the geometry simulation allows the user to switch off features that are computationally expensive in situations where they do not significantly affect the results.

The actual data from the SNO detector are written to tape in the form of packed ZEBRA banks. SNOMAN processors unpack the data and then calibrate it by applying pedestal, slope and offsets to the ADC data to produce PMT hits with corrected times and charges (other processors exist to uncalibrate and then pack the Monte Carlo data, thus allowing the whole data stream to be tested with Monte Carlo data). After the calibration processor, the data handling is identical for Monte Carlo and detector data. A number

of processors then exist to derive additional information from the PMT hit times and positions. The first type of these are called "fitters." These derive an event position and direction from the PMT data. A number of different algorithms exist for this purpose. In addition to the fitters there are processors called classifiers that derive information from the angular distribution of hits in the event. This information has been shown to be a powerful tool for discriminating between neutral-current and charged-current events [56] and for measuring the most important background events directly [57].

Once all of these processors have finished the resulting data can be viewed using two tools–the event viewer and the event analyzer. The event viewer is a graphical display of the SNO detector which displays the various detector elements and PMT hits in 3D and a number of 2D formats. The analyzer is a data-driven tool for sifting through the entries in the data structure (or through quantities derived from the entries in the data structure by one of a large number of supplied functions) to find those that satisfy either individual cuts or logical combinations of a number of cuts applied to different quantities. Any entries or quantities which pass the cuts are written as an entry in a CERNLIB HBOOK ntuple for later additional analysis with PAW [58]. A slightly unusual feature of SNO (from the point of view of a typical high-energy physics experiment) is that some events are correlated in time or position (the spallation products following a through muon, for example). This information can be extracted from the data using the time correlation processor, which allows the analyzer to combine information from different events that satisfy conditions placed on their relative time or position into a single ntuple entry.

13 Conclusion

The Sudbury Neutrino Observatory is a large, second-generation neutrino detector with active fiducial volumes consisting of 1000 tonnes of highly purified heavy water plus about 1000 tonnes of purified light water. The detector will provide high statistics data from natural neutrino sources, with an emphasis on the study of solar neutrinos from ^{8}B decay and whether or not they undergo flavor oscillations as they propagate from the core of the sun to the earth. The ability of SNO to distinguish charged-current and neutral-current neutrino interactions is unique among present-day solar neutrino detectors that are operating or under construction. SNO is also the only neutrino detector that can exclusively identify antineutrino interactions. The unusually deep location of SNO and particular attention to minimization of radioactive backgrounds makes possible high signal-to-background measurements.

A series of engineering runs to test detector performance and commission various detector systems began without water present in the detector cavity

in September, 1997. SNO was completely filled with heavy and light water on April 30, 1999, at which time full system operation commenced. The detector will be run with pure D_2O until the SNO collaboration determines that a physically interesting dataset has been accumulated. Then, the detector will be modified to enhance its neutral-current detection capabilities.

The resulting dataset should enable SNO to make a definitive measurement of the fraction of electron neutrinos in the solar neutrino flux, distinct from all previous measurements in that it will be independent of theoretical models of the sun. This and other measurements are expected to deepen the understanding of the properties of neutrinos and of the astrophysical sites from which they originate.

Acknowledgements

This research has been financially supported in Canada by the Natural Sciences and Engineering Research Council, Industry Canada, National Research Council of Canada, Northern Ontario Heritage Fund Corporation and the Province of Ontario, in the United States by the Department of Energy, and in the United Kingdom by the Science and Engineering Research Council and the Particle Physics and Astronomy Research Council. Further support was provided by INCO, Atomic Energy of Canada Limited (AECL), Agra-Monenco, Canatom, Canadian Microelectronics Corporation and Northern Telecom. The heavy water has been loaned by AECL with the cooperation of Ontario Hydro. The provision of INCO of an underground site is greatly appreciated. The collaboration wishes to express gratitude for all the support provided to make the experiment possible.

References

[1] S. Weinberg, Phys. Rev. Lett. **19** 1264 (1967); A. Salam in *Elementary Particle Theory,* ed. N. Svartholm, p. 367 (1969); S.L. Glashow, J. Iliopoulus, and L. Maiani, Phys. Rev. **D2**, 1285 (1970).

[2] L. Wolfenstein, Physical Review D **17**, 2369 (1979);
S. P. Mikheyev and A. Yu. Smirnov, Yad. Fiz. **42**, 1441 (1985) (Sov. J. Nucl. Phys. **42**, 913 (1985);
Nuovo Cimento **9C**, 17 (1986).

[3] B. T. Cleveland *et al.*, Astrophys. J. **496**, 505 (1998).

[4] Kamiokande II Collaboration, K. S. Hirata *et al.*, Physical Review Letters **65**, 1297 (1990); , 1301 (1990); **66**, 9 (1991); Physical Review D **44**, 2241 (1991);

Superkamiokande Collaboration, Y. Fukuda *et al.*, Physical Review Letters **81**, 1158 (1998).

[5] SAGE Collaboration, J. N. Abdurashitov *et al.*, Physical Review Letters **77**, 4708 (1996); astro-ph/9907113 (1999); GALLEX Collaboration, W. Hampel *et al.*, Physics Letters B **447**, 127 (1999).

[6] J. N. Bahcall, S. Basu, and M. H. Pinsonneault, Physics Letters B **433**, 1 (1998); A. S. Brun, S. Turck-Chièze, and P. Morel, Astrophys. J. **506**, 913 (1998).

[7] A. Dekok, MSc. thesis, Department of Physics, Carleton University (1996).

[8] *Design Description for the SNO SUF Plant*, R.K. Taplin et al., Sudbury Neutrino Observatory, SNO-STR-96-033 (1996).
R.K. Taplin, D. Phil. thesis, Department of Physics, Oxford University (1996).

[9] J.-X. Wang, *Data Analysis of ESC Counting for Ra and Rn*, Sudbury Neutrino Observatory, SNO-STR-95-066 (1996).
T. Anderson et al., *Recent Results on Extraction Efficiencies, Systematics, and Fines with MnO_2 Coated Beads*, Sudbury Neutrino Observatory, SNO-STR-95-022 (1995).

[10] J.-X. Wang, T. Anderson, and J.J. Simpson, Nucl. Inst. and Meth. **A421** (1999) 601.

[11] X. Zhu, M.Sc. thesis, Department of Physics, Queen's University (1993).
S. Noel, M.Sc. thesis, Department of Physics, Queen's University (1995).

[12] M.-Q. Liu, H.W. Lee and A.B. McDonald, Nucl. Inst. and Meth. **A329** (1993) 291.

[13] J. Bigu, E.D. Hallman and L. Kendrick, *Permeability of Different Materials to Radon,* SNO-STR-91-069 (1991).
M. Wojcik, Nucl Inst. and Meth. (**B61** (1991) 8.
W. Müller, thesis, University of Heidelberg (1978).

[14] ANSYS Inc., 275 Technology Drive, Connonsburge, PA 15317 (http://www.ansys.com).

[15] P. Jagam and J.J. Simpson, Nucl. Instr. and Meth. **A324** (1993) 389.

[16] C. Athanassopoulos *et al.*, Phys. Rev. C **54** (1996) 2658.

[17] MacLeod, R.W., *Evaluation of Large Area Photomultiplier Tubes for the Sudbury Neutrino Observatory,* M.Sc. thesis, Department of Physics, Queen's University (1990).

[18] C.J. Jillings et al. Nucl. Instr. and Meth. A373 (1996) 421.

[19] Jillings, C.J., *A Photomultiplier Tube Evaluation System for the Sudbury Neutrino Observatory,* M.Sc thesis, Department of Physics, Queen's University (1992).

[20] Project Notebook, Sudbury Neutrino Observatory, K.T. Lesko, Lawrence Berkeley National Laboratory, Rev. B.

[21] G. Doucas *et al.*, Nucl. Instr. Meth. **A370** (1996) 579-596.

[22] The PSUP conforms to numerous construction codes and standards. American Institute of Steel Construction Manual of Steel Construction, Allowable Stress Design, 9th edition, 1989, American Society for Testing and Materials, American National Standards Institute, ANSI Y14.5M, American Welding Society, and Lawrence Berkeley Laboratory Health and Safety Manual (Pub. 3000).

[23] H. Leung, *Tensile Creep Testing of ABS Plastic Final Report,* SNO-STR-92-055.

[24] AT&T Microelectronics, Allentown, Pennsylvania.

[25] F.M. Newcomer and R. Van Berg, *A Wide Dynamic Range Integrator-Discriminator-Timer Chip Set for PMT Applications,* IEEE Nuclear Science Symposium, Transactions on Nuclear Science, Vol. 42, No. 4, pp. 925-932, 1995.

[26] T. Ekenberg, R. Van Berg, A. Biman, R.L. Stevenson, *An Analog Memory, Time to Amplitude Converter, and Trigger Logic Chip for PMT Appplications,* IEEE Nuclear Science Symposium and Medical Imaging Conference, IEEE Conference Record, Vol. 1, pp. 30-34, 1995.

[27] Northern Telecom, Ottawa, Ontario, Canada.

[28] ZEBRA, CERN Program Library Long Writeup Q100/101, CERN, Geneva, Switzerland.

[29] T.J. Bowles *et al.*, in *Neutral-Current Detection in the Sudbury Neutrino Observatory*, Los Alamos National Laboratory, Appendix to FIN-94-ER-E324, January 31 (1992).

[30] E.L. Pasierb, Ph.D. Dissertation, University of California, Irvine, 1979.

[31] I.I. Gurevich *et al.*, I.V. Kurchatov Institute of Atomic Energy Preprint IAE-4986/2 (1989).

[32] G.S. Vidyakin *et al.*, JETP Lett. **59** (1994) 364.

[33] Y. Fukuda *et al.*, Phys. Rev. Lett. 81, 1185 (1998).

[34] K. Kubodera and S. Nozawa, Int. J. Modern Phys. **E3** (1994) 101.

[35] Nemasoft Corporation, 55 West Street, Walpole, MA 02081 USA.

[36] Sciemetric Instruments Inc., 27 Northside Road, Nepean, ON K2H 8S1, Canada.

[37] R.J. Ford, *SNO N_2/Dye Laser and Fibre Optic Diffuser Ball System Manual*, Sudbury Neutrino Observatory, SNO-STR-96-056 (1997).
R.J. Ford, *Nitrogen/Dye Laser System for the Optical Calibration of SNO*, M.Sc. thesis, Department of Physics, Queen's University (1993).

[38] S. Hilgenfeldt, S. Grossman, and D. Lohse, Nature **398** (1999) 402.

[39] B.P. Barber *et al*, Phys. Rep. **281** (1997) 65.

[40] Douglas McDonald, *Studies of the Sudbury Neutrino Observatory Detector and Sonoluminescence Using a Sonoluminescent Source*, Ph.D. thesis, Department of Physics and Astronomy, University of Pennsylvania (1999).

[41] Y. Sato, N. Takahashi and S. Sato, Jpn. J. Appl. Phys. **35**, 7A (1996) L838.

[42] B. Sur *et al*, Bull. Am. Phys. Soc. **39**, (1994) 1389.

E.B. Norman and B. Sur, *^{17}N: A Tagged Neutron Source for SNO*, Sudbury Neutrino Observatory, SNO-STR-94-037 (1994).

B. Sur and E.D. Earle, *Gas Transport Calibration System for SNO: a preliminary design document*, Sudbury Neutrino Observatory, SNO-STR-95-053 (1995).

B. Sur, E.D. Earle, R. Deal and E. Gaudette, *^{8}Li: A Beta Calibration Source for SNO*, Sudbury Neutrino Observatory, SNO-STR-95-054 (1995).

J.N. Bahcall and E. Lisi, Phys. Rev. **D54**, (1996) 5417.

A. Hamer and B. Sur, *Targets for the ^{16}N Calibration Source*, Sudbury Neutrino Observatory, SNO-STR-97-033 (1997).

G. Jonkmans, I.S. Towner and B. Sur, Phys. Rev. **C58** (1998) 1278.

[43] A.W.P. Poon *et al.* in Particles and Cosmology, ed. E.N. Alexeev, V.A. Matveev, Kh. S. Nirov, V.A. Rubakov, World Scientific, page 248 (1996); *Energy Calibration of the Sudbury Neutrino Observatory Using Monoenergetic Gamma-Ray Sources*, A.W.P.Poon, Ph.D. thesis, Department of Physics, University of British Columbia, 1998; A.W.P. Poon *et al.*, *A Compact $^{3}H(p,\gamma)^{4}He$ 19.8-MeV Gamma-Ray Source for Energy Calibration at the Sudbury Neutrino Observatory*, submitted to Nucl. Inst. Meth. A. A.W.P. Poon, *Energy Calibration of the Sudbury Neutrino Observatory Using Monoenergetic Gamma-Ray Sources*, Ph.D. dissertation, University of British Columbia (1998).

[44] F. Dalnoki-Veress and C.K. Hargrove, *A Proportional Counter to Calibrate SNO Backgrounds*, Sudbury Neutrino Observatory, SNO-STR-97-052 (1997).

F. Dalnoki-Veress, *Investigation of the Triggered Source Technique for the Calibration of SNO*, M.Sc. thesis, Department of Physics, Carleton University (1996).

C.K. Hargrove, Ira Blevis and E. Bonvin, *Coincidence Measurements of SNO Background Spectra with a Proportional Counter*, Sudbury Neutrino Observatory, SNO-STR-94 (1994).

[45] R.J. Ford, *Fitting Optical Constants in SNO Using a Pulsed N_2/Dye Laser*, Sudbury Neutrino Observatory, SNO-STR-96-055 (1996).

S. Biller and R.J. Ford, *Optical Calibration Strategies*, Sudbury Neutrino Observatory, SNO-STR-96 (1996).

[46] C.F. Bohren and D.R. Huffman, *Absorption and Scattering of Light by Small Particles*, Wiley, NY (1983).

[47] C. Waltham *et al*, Appl. Opt. **33**, 31 (1994) 7536.

[48] An application of this thickness monitoring technique has recently been patented (U.S. Patent No. 5,862,199; *Method and Apparatus for Measuring Thickness of Paint Layers on Substrates Using Backscattering of X-Rays*) and commercial development of the monitor is in progress.

[49] W.R. Nelson, H. Hirayama and D.W.O. Rogers, *The EGS4 code system*, SLAC report 265 (1985).

[50] *MCNP4A, A Monte Carlo N-Particle Transport Code System*, Radiation Shielding Information Center, Los Alamos National Laboratory, Nov. 1993 (unpublished).

[51] *CN/ASD, Geant Detector Description and Simulation Tool*, CERN (1994) (unpublished).

[52] N. Hata *et al.* Phys. Rev. D **50** (1994) 632.

[53] M.G. Bowler, Nucl. Inst. Meth. **A378** (1996) 463.

M.G. Bowler and M.D. Lay, Nucl. Instr. Meth. **A378** (1996) 468.

[54] M. D. Lay, D. Phil. thesis, Department of Physics, Oxford University (1994).

[55] M. J. Lyon, D. Phil. thesis, Department of Physics, Oxford University (1996).

[56] S. J. Brice, D. Phil. thesis, Department of Physics, Oxford University (1996).

[57] Xin Chen, D. Phil. thesis, Department of Physics, Oxford University (1997).

[58] *CN/ASD, Physicist Analysis Workstation*, CERN (1998) (unpublished).